# Quantitative proteomics and phosphoproteomics analyses identify sex-biased protein ontologies of *S. japonicum*

Chuantao Fang[a], Bikash R. Giri[a ʒ], Guofeng Cheng[a,b]*

[a] Shanghai Tenth People's Hospital, Institute for Infectious Diseases and Vaccine Development, Tongji University School of Medicine, Shanghai 200311, China; Clinical Center for Brain and Spinal Cord Research, Tongji University, Shanghai 200092, China; Affiliated Shanghai Blue Cross Brain hospital, School of Medicine, Tongji University, Shanghai 200020, China

[b] Shanghai Veterinary Research Institute, Chinese Academy of Agricultural Sciences, Key Laboratory of Animal Parasitology of Ministry of Agriculture and Rural Affairs, Shanghai 200241, China

* To whom correspondence may be addressed: Guofeng Cheng, Ph.D., Email: chengguofeng@tongji.edu.cn

ʒ present address: Dept. of Zoology, KKS Women's College, Manikhamb, Balaore 756003, Odisha, India

**Manuscript information**

**Words: 5266**

**References:53**

**Tables: 3**

**Figures: 4**

**Supplementary figures: 4**

**Supplementary tables: 8**

**Article title (below 100 characters) :** Quantitative proteomics and phosphoproteomics analyses identify sex-biased protein ontologies of *S. japonicum*

**Running title (below 50 characters):** Proteome and phosphoproteome of *S. japonicum*

**Keywords (5 words) :** *Schistosoma japonicum*; phosphoprotein; signal transduction; development; sexual maturation

**Words in Abstract:** 231

**Abstract**

*Schistosoma japonicum* (*S. japonicum*) is one of the major causative agents of human schistosomiasis in Asia. Identification of differentially expressed proteins (DEPs) between male and female worms could reveal the critical signaling pathways that are involved in sexual maturation and egg production. In the study, quantitative proteome and phosphoproteome profiles were obtained from adult male and female worms of *S. japoncum*. A total of 2,710 unique proteins, including 2,055 proteins and 924 phosphorylated proteins were identified. Combined with the analysis of the RNA sequencing dataset, we found 252 (~12.5%) non-phos and 209 (11.7%) phosphorylated DEPs between males and females. Notably, only 1.2% of the non-phosphorylated DEPs exhibited corresponding mRNA-level changes. Next, several identified DEPs were further corroborated to be involved in sex-biased biological processes including vitellocyte development, oviposition, and mobility by RNA interference. Furthermore, we annotated 96 kinases of *S. japonicum* based on the obtained phosphorylated proteins, of which CMGC/MAPK, Atypical/RIO, are significantly activated in males, while CAMK/CAMKL, AGC/DMPK, and STE/STE7 in females. Finally, the potential drugs targeting these kinases were determined in silico, resulting in the identification of 28 *S. japonicum* kinases as potentially targetable by 30 FDA-approved drugs. Overall, our study provided a collection of evidence-based proteomic and phosphoproteomic resources of *S. japonicum*, and identified sex-biased proteins, phosphopeptides, and kinases in adult female and male worms, which could serve as potentially effective targets for developing novel interventions against schistosomiasis.

**Keywords:** *Schistosoma japonicum*; phosphoprotein; signal transduction; development; sexual maturation.

## Introduction

Schistosomes are blood-dwelling helminth parasites that can infect humans and certain mammals worldwide [1]. Schistosomiasis caused by schistosome infections afflicted approximately 230 million individuals in 78 nations, representing a significant global health problem [2]. It accounts for an estimated annual mortality of 200,000 cases and contributes 3.3 million disability-adjusted life years (DALYs) to the global disease burden [2-4]. In Asia, *Schistosoma japonicum* (*S. japonicum*) infection was frequently found in China, Philippines, and a small area of Indonesia [5]. Currently, praziquantel is the only drug of choice for schistosomiasis treatment although it's ineffective for juvenile worms, of which the long-term usage, unfortunately, was challenged due to the concerns of drug resistance [6, 7]. In the etiology of schistosomiasis, the main pathogenic manifestations and disease transmission are directly mediated by oviposition from sexually matured worm pairs, which implies multiple potential therapeutic intervention points. However, translational exploitation of these targets remains unrealized due to insufficient elucidation of the underlying molecular mechanisms governing parasite development and egg production.

During the complex life cycle, schistosomes undergo multiple morphological changes and sexual maturation starts with a continuous pairing of males with females to ensure reproductive development [8, 9]. Previous studies demonstrated that physical and chemical intersexual interactions could significantly enhance reproductive development and egg production in schistosomes [10]. Consequently, elucidating the molecular mechanisms governing sex-biased developmental processes represents a critical research imperative. In 2022, the proteomic profiles of unisexual- and bisexual-infected *S. japonicum* male worms revealed 674 differentially expressed proteins (DEPs) across several developmental time points [11], showing that a large number of proteins were altered under these processes. Moreover, several studies identified protein phosphorylation as a pivotal post-translational regulatory mechanism that coordinates signaling cascades, thereby modulating essential biological processes, including parasitic growth and reproduction [12, 13]. For instance, protein phosphorylation was shown to play a critical role in the transformation of cercariae to schistosomula, a key step for host infectivity [14]. Similarly, Ressurreicao and coworkers demonstrated that heightened ERK and PKC activation within the cephalic ganglia of praziquantel-treated specimens correlates with tegumental and excretory system modifications, contributing to *S. mansoni* homeostasis [13]. In *S. japonicum*, Luo and coworkers identified 127 distinct phosphorylation sites in 92 proteins, of which 30 were phosphorylated, including signaling molecules like 14-3-3 and HSP90 [15]. These studies highlight the critical roles of protein phosphorylation modification in schistosome biology; however, whether there is a divergence in phosphoproteome between male and female worms remains unclear.

In the present study, we employed an integrated iTRAQ quantitative proteomic and phosphoproteomic methodology to pursue two primary research goals: 1) construct a systematic protein-level profile of *S. japonicum*, and 2) comprehensively delineate sexually dimorphic protein and phosphoprotein expression profiles between adult male and female worms. In parallel, functional experiments were conducted to validate the biological relevance of prioritized molecular targets. Kinase activity profiling was conducted through a tailored Gene Set Variation Analysis (GSVA) algorithm, leveraging curated protein interaction networks from the STRING database as molecular interaction frameworks. This multidimensional analytical paradigm generated three pivotal outcomes: 1) a comprehensive quantitative proteomic/phosphoproteomic dataset for *S. japonicum*, 2) identification of sex-biased different proteins and phosphoproteins, and 3) characterization of sex-biased different kinase activation states.

## Results

### Overview of iBQP and iBQPP protein profiles

Adult male and female *S. japonicum* at 35 days post-infection (dpi) were profiled using integrated iTRAQ-based quantitative proteomic (iBQP) and phosphoproteomic (iBQPP) approaches as outlined in the workflow (**Fig. 1A**). Briefly, protein lysates from adult male and female worms were independently prepared and tryptically digested to generate peptides. The resultant peptides underwent 8-plex iTRAQ isotopic labeling, with subsequent phosphopeptide enrichment via titanium dioxide ($TiO_2$) affinity chromatography. Triplicate biological replicates were carried out by Q-Exactive liquid chromatography-tandem mass spectrometry (LC-MS/MS) system following quality control validation.

According to the Mascot program searching, we yielded 317,107 raw spectra in total, which were matched to an average of 37,690 spectra and 10,046 high-scoring unique peptides after peptide retrieval using *S. japonicum* proteome database (**Supplementary Table 1**). This resulted in the identification of 2,055 non-redundant proteins with 21.6% sequence coverage (**Fig. 1B**, **Supplementary Tables 1-2**). Database annotation revealed 99.6% (2,047/2,055) of proteins matched UniProtKB entries, while 0.4% represented gene products from previous genome annotations (ASM15177v1 genome assembly) (**Fig. 1C**). Chromosomal mapping demonstrated non-biased protein distribution across all nine chromosomes, exhibiting congruence with genomic gene density patterns (**Fig. 1D**).

Gene Ontology (GO) enrichment analysis of high-abundance proteins (defined as >50% sequence coverage) revealed significant associations with: 1) biological processes: microtubule-based motility (GO:0007018), proteolytic regulation (GO:0006508), organelle reorganization (GO:0006996), and chaperone-mediated folding (GO:0061077); 2) cellular components: cytoskeletal architecture (GO:0005856), catalytic complexes (GO:0098783), and microtubular networks (GO:0005874); 3) molecular functions: GTPase activity (GO:0003924), ATP-dependent catalytic activity (GO:0140657), and ATP hydrolysis-coupled transport (GO:0043461) (**Fig. 1E and S1A**). Consistently, Kyoto Encyclopedia of Genes and Genomes (KEGG) pathway analysis corroborated these findings, showing enrichment in Salmonella infection signaling (sja05132), motor protein interactions (sja04810), and tight junction regulation (sja04530) (**Supplementary Fig. S1A**). Collectively, the proteome landscape captures the full spectrum of molecular characteristics in adult worms.

### Quantitative description and functional enrichment analysis of DEPs between males and females

To systematically investigate sex-biased proteomic profiles in *S. japonicum*, we conducted principal component analysis (PCA) on global protein expression data, revealing that primary variance (PC1) predominantly originated from sexual dimorphism (**Fig. S2A**). This sexual divergence was corroborated by clustering analysis of protein expression (or proteomic profile), with clear segregation between male and female worms in the heatmap visualization (**Fig. 2A**). Integration of our proteomic dataset with publicly available transcriptomic data (PRJNA428445) [16] revealed limited concordance between protein abundance and corresponding mRNA levels (**Fig. S2B**), suggesting substantial post-transcriptional regulatory mechanisms governing protein expressions. Meanwhile, the comparative analysis demonstrated minimal overlap between differentially expressed proteins (DEPs, n=252) and differentially expressed genes (DEGs), with only three genes (EWB00_003121, EWB00_001015, EWB00_009171) exhibiting concurrent differential expression at both levels (**Fig. 2B**, **Supplementary Table 3**). Conversely, the majority of sex-biased DEGs showed no corresponding proteomic alterations (**Fig. S2C-E**; **Supplementary Table 4**). These findings underscore the necessity of proteomic profiling to comprehensively characterize cellular phenotype.

Gene Set Enrichment Analysis (GSEA) of sex-biased proteins revealed distinct functional specializations. For instance, female-enriched proteins predominantly associated with metabolic processes, particularly protein catabolism, proteolysis, etc, while male-enriched proteins associated with cytoskeletal organization and contractile fiber components (**Fig. 2C**). Molecular function analysis identified peptidase activities (both exopeptidase and endopeptidase) as female-specific, contrasting with male-biased transferase activities (**Fig. 2C**). KEGG pathway analysis further revealed sexual dimorphism: vasopressin-regulated water reabsorption pathways (ko04962) were male-enriched, while females showed enrichment in autophagy (ko04140), apoptosis (ko04210), and lysosomal pathways (ko04142) (**Fig. 2C**). Furthermore, protein-protein interaction network analysis (STRING v11.5) of DEPs identified three functionally significant modules: cytoskeletal remodeling complexes, vacuolar ATPase assemblies, and signal transduction cascades (**Fig. 2D**).

To further validate the functional roles of the identified DEPs, we selected two female-enriched genes, *Ft* (EWB00-000538) and *Catb1* (EWB00-007550), which are putatively expressed in gut and vitellocyte cells according to the single-cell RNA sequencing data of *S. mansoni* [17](**Fig. 2E**). Functional validation demonstrated that silencing these two genes resulted in significant impairment of the vitellocyte development and oviposition in female worms (**Fig. 2F and 2G**). Mobility is physiologically linked to mating stability and egg production during the sexual maturation of schistosomes [18]. Interestingly, we observed that the knockdown of two other sex-biased genes (*Mcm4* and *Agp*) effectively impacted worm mobility, and also influenced the oviposition of female worms (**Fig. 2H-I and S2F**). These findings collectively demonstrate that proteomic profiling provides critical insights into sex-biased molecular mechanisms governing schistosome biology.

## Differentially expressed phosphorylated proteins between males and females.

Phosphorylation, as the most prevalent post-translational modification in eukaryotic species, serves as a critical regulatory mechanism across diverse biological pathways. Despite its evolutionary conservation in higher organisms, the phosphoproteomic landscape and its functional implications remain poorly characterized in *S. japonicum*. To address this knowledge gap, we performed a comparative phosphoproteomic analysis between male and female worms. Initial quality assessments revealed statistically comparable parameters in intersex comparative phosphoproteomic datasets, including total peptide counts, peptide length distributions, and quantitative intensity profiles (**Fig. S3A-C**).

Through integrated annotation using the *S. japonicum* proteome database (Anhui, AH and Fudan, FD version) supplemented with UniProt, we identified 869 phosphoproteins with high confidence (**Fig. 3A, Supplementary Table 5)**. Notably, only 214 proteins (24.7% of total phosphoproteins) exhibited overlap with the characterized proteomic datasets, indicating that 75.3% of phosphorylation events occur on proteins undetected in conventional proteomic analyses (**Fig. 3A**). Site-specific analysis demonstrated rigorous localization reliability, with >90% of phosphorylation sites (both singly- and multiply-phosphorylated peptides) achieving a posterior probability threshold >0.8 (**Fig. 3B**). Among these high-confidence sites, most peptides possessed 1-2 serine or threonine modification (**Fig. 3C**). PCA analysis revealed that sexual dimorphism explained most of phosphoproteomic variance (PC1, **Fig. 3D**). Hierarchical clustering of phosphoprotein expression levels further confirmed significant intersex divergence (**Fig. 3E, Table 1 and 2, Supplementary Table 6**). These findings collectively implicate protein phosphorylation as a potential molecular determinant in sexually dimorphic physiological processes in *S. japonicum*.

To elucidate the biological significance of protein phosphorylation in *S. japonicum*, we performed systematic kinase prediction for serine/threonine/serine-threonine (S/T/ST) phosphorylation sites using KinasePhos3.0, a comprehensive computational tool employing profile hidden Markov models (HMMs) for kinase-specific phosphorylation site prediction [19]. Applying a stringent probability threshold (>0.95) of being a real modification, we identified 1,428 serine, 1,501 serine-threonine, and 222 threonine phosphorylation sites, respectively (**Fig. 3F**). Functional enrichment analysis revealed these phosphoproteins predominantly participate in 1) biological processes: protein catabolic regulation, phosphorylation cascades, and MAPK signaling pathways; 2) cellular components: supramolecular polymers and microtubule networks; 3) molecular functions: cytoskeletal structural maintenance, serine/threonine/tyrosine kinase activity, and MAP kinase activation (**Fig. 3G**).

Leveraging the S/T/ST phosphorylation sites, subsequent kinome prediction utilizing GPS6.0 software [20], an enhanced algorithm for kinase-specific phosphorylation site identification, demonstrated preferential modification by three major kinase families: AGC (protein kinases C and A), CAMK (calcium/calmodulin-dependent kinases including CAMKL and CAMK2), and CMGC (cyclin-dependent kinases and MAP kinases). Quantitative distribution across kinase families was quite balanced (**Supplementary Fig. S3D**). Motif analysis via MEME Suite identified several conserved phosphorylation motifs, notably STE20, CDK, MAPK, and CAMKL signatures (**Supplementary Fig. S4**). Collectively, these findings suggest a complex, phosphorylation-driven regulatory network in *S. japonicum*, orchestrating developmental processes and cellular architecture homeostasis via sex-biased kinase families.

## Differential kinase activity between males and females

To comprehensively investigate kinase signaling pathways governing *S. japonicum* development, we developed a

computational framework for kinase activity quantification through quantitative phosphorylated substrate profiling. The methodological workflow (**Fig. 4A**) comprises three principal steps: 1) database curation of 29,803 *S. japonicum* protein sequences from UniProt, followed by homology-based prediction of 96 conserved kinases through Diamond [21] alignment (identity threshold >30%) against *Caenorhabditis elegans* kinase orthologs; 2) construction of kinase-substrate interaction networks through the integration of functional and physical protein-protein interaction data; 3) quantitative kinase activity inference via GSVA applied to phosphoproteome profiles mapped against curated substrate gene sets.

Differential analysis of kinase activity revealed significant sexual dimorphism in kinase activity profiles, with pronounced differential activation patterns between male and female worms (**Fig. 4B-C**). Sex-biased kinase enrichment analysis demonstrated male-biased activation of CMGC/MAPK, Atypical/RIO, and STE/STE Unique kinase families, contrasting with female-prevalent activity in CAMK/CAMKL, AGC/DMPK, and STE/STE7 clusters (**Fig. 4D**). Subsequent GO enrichment analysis of differentially active kinases identified significant associations with essential biological processes including protein metabolic process, phosphorylation regulation, etc, and molecular functions encompassing serine/threonine kinase catalytic activity (**Fig. 4E**). Through systematic interrogation of the DGIdb 5.0 pharmacogenomic database [22], we identified 28 *S. japonicum* kinases (including AKT3, CDKs, and MAPKs orthologs) exhibiting >60% sequence identity with human drug-targetable kinases (**Table 3 and Supplementary Table 8**). Meanwhile, 30 FDA-approved therapeutic agents are available for the homologous human kinases, which may be candidates for developing drugs against schistosomiasis (**Table 3**).

## Discussion

In recent years, multi-omics methodologies (e.g., proteomics and transcriptomics) have been systematically employed in schistosome research to advance gene annotation, spatiotemporal gene expression profiling, etc. Notably, parasite eggs constitute the main pathogenic drivers of schistosomiasis pathogenesis. During sexual maturation and oviposition, male and female parasites fulfill distinct yet complementary biological roles, suggesting potential divergence in their protein ontologies and functional repertoires. To elucidate the molecular mechanisms underlying these processes, we conducted an iTRAQ-based quantitative proteomic and phosphoproteomic profiling to systematically characterize sex-biased protein and phosphoprotein profiles in adult *S. japonicum*.

Our analytical workflow successfully identified 10,046 non-phosphorylated peptides corresponding to 2,055 distinct proteins, establishing a comprehensive baseline proteomic inventory. Unexpectedly, cross-platform analysis revealed a remarkably low correlation coefficient (<0.4) between proteomic and transcriptomic profiles, indicating that post-transcriptional regulatory mechanisms could predominantly govern final protein expression levels in this biological system. Meanwhile, our phosphoproteomic analysis identified 1,833 phosphopeptides mapping to 869 phosphoproteins, with notable heterogeneity observed between sexes. The combined proteomic approaches enabled the identification of 2,710 unique proteins, representing a large expansion of the documented *S. japonicum* proteome. Furthermore, functional enrichment analysis demonstrated that highly abundant proteins were significantly associated with essential cellular processes including cytoskeletal reorganization, microtubule dynamics, intercellular communication, and proteolytic regulation, corroborating and extending previous investigations in schistosome biology [11]. Collectively, the comprehensive dataset generated through this study establishes a critical foundation for understanding phosphorylated protein mediated regulation of reproductive biology in *S. japonicum*.

After comprehensive proteomic profiling, we conducted a comparative analysis of sexually dimorphic protein expression in adult *S. japonicum*. We identified 252 DEPs between female and male adults, representing approximately 12.5% of the total identified proteome. After integrating with prior transcriptomic data, we found a minimal concordance between DEPs and DEGs, with only 1.2% of protein-level alterations corresponding to transcriptional changes. This cue, pronounced post-transcriptional regulatory divergence, underscores the necessity of direct proteomic investigation for accurate characterization of functional molecular phenotypes. Protein interaction network modeling demonstrated significant interconnectivity among DEPs associated with cytoskeletal dynamics, vesicular trafficking, and signal transduction cascades. Functional annotation of female-enriched DEPs revealed significant enrichment in biosynthetic processes, including cellular metabolism, protein modification, and proteolytic activity, consistent with the elevated metabolic demands of oogenesis [23]. Conversely, male-specific proteins exhibited enrichment in structural components, particularly cytoskeletal organization, and contractile apparatus formation, mechanistically supporting their characteristic gynecophoral canal morphology essential for pairing. Furthermore, we identified 209 differentially phosphorylated proteins (11.7% of 1,792 phosphosites), with functional clustering in regulatory pathways including protein catabolism, MAP kinase signaling, chromatin remodeling, and cellular junction assembly. These conserved phosphorylated protein mediated regulatory networks exhibit evolutionary conservation across metazoans [23, 24], suggesting shared post-translational regulatory mechanisms in *S. japonicum.*

Functional validation through RNA interference targeting female-enriched genes EWB00-000538 and EWB00-007550 revealed significant impairment of vitellocyte development and oviposition for female worms. EWB00-007550 encodes a protein named ferritin in *S. japonicum*. In 2022, Zeng et al. found that the ability of egg production was significantly reduced after ferritin knockdown [25]. EWB00-000538 encodes a protein named cathepsin B-like cysteine proteinase isoform 1(*Catb1*), mainly expressed in gut cells. Cathepsin, a cysteine protease localized within subcellular endosomal and lysosomal compartments, is involved in the turnover of intracellular and extracellular proteins to mediate processes including apoptosis, pyroptosis, ferroptosis, necroptosis, and autophagic cell death [26]. Previously, Wang et al., reported that mobility is physiologically linked to mating stability and egg production during sexual maturation [18]. Recently, Piao et al., also found that TH (Tyrosine hydroxylase, an enzyme mediating biosynthesis of neurotransmitter) is expressed in the head, tegument, and intestinal intima, and immunization with recombinant SjTH has been shown to reduce the worm and egg burden of the host [27]. Consistently, interfering EWB00-001858 and EWB00-010322 expression significantly decreased worm motility

and oviposition, showing the potential contribution of mobility to worm maturation. Collectively, our multi-omics integration establishes the proteome-defined DEP repertoire as a critical resource for elucidating sex-biased molecular adaptations in schistosome biology.

Next, we developed a computational framework for kinase activity quantification through quantitative phosphorylated substrate profiling by the following paradigm steps: 1) kinase annotation using homology-based prediction through protein sequence alignment, 2) construction of kinase-substrate interaction networks (or gene sets) through the integration of functional and physical protein-protein interaction data; 3) quantitative kinase activity inference via GSVA-based algorithm using phosphoproteomic profiles mapped against curated substrate gene sets. By bridging protein-protein interaction data (such as the STRING database) with phosphoproteomic data, our integrative approach provides a systematic strategy to overcome the inherent challenges of studying the kinome of non-model organisms with limited prior annotations. These methodological advancements collectively accelerate therapeutic discovery by pinpointing kinase-mediated developmental vulnerabilities that could be targeted by selective inhibitors.

The pivotal roles of kinases in schistosomes have been to some extent studied, revealing conserved and parasite-specific kinases that regulate critical developmental pathways, particularly in signaling, growth, differentiation, and reproductive processes. For instance, protein kinases (PKs), including serine/threonine kinases (e.g., PLKs, MAPKs, etc) and protein tyrosine kinases (PTKs), are essential for processes like gonad maturation, pairing-dependent sexual differentiation, and host-parasite interactions [16, 28]. Cellular tyrosine kinases (CTKs), such as SmTK3, are implicated in female gonad differentiation and signaling cascades [29, 30]. RNA interference and pharmacological inhibition experiments have validated kinases like PKC, ERK, and FAK as potential drug targets [31, 32]. In the current study, DGIdb 5.0, a pharmacogenomic database, was used in our screening step, which directly prioritized the 30 FDA-approved kinase inhibitors. Among them, Chloroquine, a 4-aminoquinoline derivative, has been extensively employed for over seven decades as a frontline antimalarial agent, demonstrating efficacy against *Plasmodium falciparum* and *Plasmodium berghei* strains [33]. Its mechanism involves accumulation within the acidic digestive vacuoles of intraerythrocytic malaria parasites. Next, Lamivudine, a synthetic cytosine nucleoside analog, exhibits robust therapeutic efficacy and favorable tolerability profiles in patients with chronic hepatitis B virus infection [34, 35]. This compound functions as a viral DNA chain terminator through competitive inhibition of reverse transcriptase enzymatic activity. Furthermore, lamivudine interacts with kinase domains, including those of EGFR, RIPK1, and RIPK3, implicating its role in the regulation of necroptosis and suggesting putative antineoplastic mechanisms [36]. In 2020, Melissa and coworkers demonstrated that lapatinib has potent bioactive properties against adult *S. mansoni* [37]. Investigations by Fatemeh and coworkers revealed that topical administration of 0.1% cantharidin over two weeks achieves marked therapeutic efficacy against cutaneous leishmaniasis in murine models [38]. Eman and coworkers elucidated cisplatin's anti-schistosomal activity, evidenced by tegumental damage, reduced anti-schistosomal IgG levels, and decreased egg burden, among other effects [39]. Overall, these studies corroborated the credibility of our findings regarding our computational framework to identify effective inhibitors targeting *S. japonicum* kinases. Whereas, there are also challenges regarding side effects when developing kinase inhibitors targeting parasitic lesions due to selectivity concerns of the leading candidates. Therefore, optimization and modification steps may improve to exploit structural differences in parasite kinase active sites [40], to screen of FDA-approved kinase inhibitors against parasite-specific kinases [41], and to focus on essential parasite-specific kinases with unique structural features [42, 43].

In summary, our study provides: 1) a comprehensive atlas of sex-biased proteomes and phosphoproteomes; 2) mechanistic insights into post-translational regulation of reproductive biology; 3) a computational framework for kinase activity inference. These findings establish foundational insights into molecular determinants of sexual maturation, intersexual interaction, and oviposition in *S. japonicum*, with broader implications for targeted anti-helminthic strategies.

302 **Materials and Methods**
303
304 Parasite infection and sample collection
305 The life cycles of *S. japonicum* (Anhui isolate) were maintained using New Zealand rabbits and *Oncomelania hapensis* at the
306 Shanghai Veterinary Research Institute of the Chinese Academy of Agricultural Sciences and Tongji University. In the
307 infection, ~1500 high-activity *S. japonicum* cercariae were infected in New Zealand rabbits via the skin of the abdomen. At
308 35 days post-infection (dpi), adult schistosomes were isolated from the hepatic portal vein of the infected rabbits via the
309 perfusion methods. After a brief culture at 37° C for 4 hrs, the separated female and male worms were manually collected
310 and subjected to protein extraction, respectively. The collected worms were snap-frozen and then stored in liquid nitrogen for
311 further experiments.
312
313 Protein extraction
314 Proteins were extracted following a previously described protocol with brief modifications [44]. Briefly, ~50 mg (adult
315 female/male schistosomes) fresh or liquid nitrogen frozen parasite samples were homogenized in 500μL lysis buffer
316 (containing 4% SDS, 1 mM DTT, 150 mM Tris-HCl pH8.0) using a Dounce homogenizer. The obtained lysates were heated
317 at 100° C block for 5 min, and subjected to Ultrasonic disruption with a program of repeated 10 times with 15 s intervals.
318 Next, the lysates were further heated as before and then were centrifuged at 10,000 g for 10 min to remove cell debris or
319 tissue. Finally, the protein samples were quantified using a BCA protein assay kit (Cat: 23225, Thermo Scientific) and stored
320 at -80° C for further use.
321
322 Protein digestion and iTRAQ labeling
323 Protein digestion was performed according to the FASP procedure described by Wiśniewski et al [44]. Briefly, 200μg proteins
324 of each sample were incorporated into 30μl SDT buffer (containing 4% SDS, 100 mM DTT, 150 mM Tris-HCl pH 8.0). Small
325 molecules and detergents (e.g. DTT) in protein lysates were removed by repeated ultrafiltration (Pall units, 10 kD) using UA
326 buffer (containing 8M Urea, 150mM Tris-HCl pH 8.0). Then, the samples were added with 100 μl 0.05M iodoacetamide in
327 UA buffer to block reduced cysteine residues, and incubated in darkness for 20 min. Filters were washed twice using 100 μl
328 UA buffer three times and then 100 μl DS buffer (50 mM triethylammoniumbicarbonate at pH 8.5). Finally, the protein
329 suspensions were digested into peptides with 2 μg trypsin (Promega) in 40 μl DS buffer at 37°C. The peptide content was
330 estimated by UV light spectral density at 280 nm.
331
332 The obtained peptide samples were labeled using the 8-plex iTRAQ (Isobaric Tags for Relative and Absolute Quantitation)
333 reagent following the manufacturer's instructions (Cat: 4352135, Sigma). Each peptide sample was added with 70 μl of
334 ethanol-dissolved iTRAQ reagent, and labeled as Male-R1-113, Male-R2-114, Male-R3-115, Female-R1-116, Female-R2-
335 117, and Female-R3-118 for the further vacuum dried.
336
337 Phosphopeptide enrichment using $TiO_2$ breads
338 The four-plex iTRAQ-labeled peptides were subjected to phosphopeptide enrichment using $TiO_2$ beads following the
339 previously described protocol [45]. The trypsin-digested peptide mixture was diluted with 500 μL commercial loading buffer
340 and added to the $TiO_2$ beads. After shaking for 40 minutes, the $TiO_2$ beads were packed into a GELoader tip (Cat: Z317047
341 Eppendorf, Hamburg, Germany). The column was washed three times with 50μl washing buffer I (30% ACN and 3% TFA)
342 and then three times with 50μl washing buffer II (80% ACN and 0.3% TFA). The bound peptides were eluted with 50μl
343 $NH_4OH$, pH 10.5, and then vacuum freeze-dried. The lyophilized phosphopeptides were dissolved in 0.1% formic acid for
344 MS analysis.
345
346 Liquid chromatography-tandem mass spectrometry (LC-MS/MS) analysis
347 LC-MS/MS for phosphopeptide samples was executed using an automated Easy-nLC 1000 apparatus interfaced with a Q-
348 Exactive mass spectrometer (Cat:IQLAAEGAAPFALGMAZR, Thermo Fisher Scientific). Briefly, 5 μL of the
349 phosphopeptides solution was amalgamated with 15 μL of 0.1% (v/v) trifluoroacetic acid, after which 10 μL of the solution
350 blend was introduced for LC-MS/MS scrutiny using a Q-Exactive MS (Thermo Finnigan). A pre-column (20mm×100μm;

5μM-C18) and an analytical column (250 mm×75μm; 3 μM-C18) were employed (Thermo Fisher Scientific) with mobile phases A (0.1% formic acid in water) and B (0.1% formic acid in 84% ACN). The phosphopeptides were fractionated at a flow rate of 250 nL/min utilizing the following gradient: 0-55 % mobile phase B from 0-220 min, 55-100% mobile phase B from 220-228 min, and 100% mobile phase B from 228–240 min.

For MS analysis, peptides were scrutinized in positive ion mode. MS spectra were acquired utilizing a data-dependent top10 methodology dynamically selecting the most abundant precursor ions from the survey scan (300-1800 m/z) for HCD fragmentation. The determination of the target value is predicated on predictive Automatic Gain Control (pAGC). Dynamic exclusion duration was 40.0s. Survey scans were acquired at a resolution of 70,000 at m/z 200 and the resolution for HCD spectra was set to 17,500 at m/z 200. The normalized collision energy was 27eV and the under-fill ratio, which stipulates the minimum percentage of the target value likely to be attained at maximum fill time, was defined as 0.1%. The instrument was operated with peptide recognition mode enabled. Data-dependent mass spectra were acquired for 240 min. The full MS surveys were collated over a mass-to-charge ratio (m/z) range of 300–1,800, with the resolution set to 70,000 at m/z 200. For MS/MS, we utilized a resolution of 17,500 at m/z 200, with an isolation window of 2 m/z.

## Protein identification and data analysis

Both non-phos protein and phosphoproteins were identified and quantified using the Mascot search engine (version 2.2, Matrix Science, Boston, MA, USA) and Proteome Discoverer (version 1.3, Thermo Fisher Scientific) against a database based on two combined databases derived from *S. japonicum* NCBI (51,526 entries) and the *S. japonicum* protein database (LSBI-Sjr, 12657 sequences; 4929382 residues) (http://lifecenter.sgst.cn/schistosoma/) [46-48]. In detail, the raw files were analyzed individually with Mascot 2.2 with the following settings: 1) only of tryptic peptides with two missed cleavages; 2) peptide mass tolerance of ± 20 ppm; and 3) fragment mass tolerance = 0.1 Da. In the quantification using Proteome Discoverer 1.3, the peak intensity of each expected iTRAQ reporter ion was analyzed with parameters: 1) unique peptides with false discovery rate (FDR)⩽0.01; 2) excluding all quantification values without quantification channels, normalize on protein median, normalize all peptide ratios by the median protein ratio; and 3) median protein ratio = 1 after normalization [48]. For each phosphorylation site on the phosphopeptides, the probability phosphorylation site was set to >75%, and the phosphorylation site score was >50 [49].

MS/MS spectra were searched using the Mascot 2.2 engine against the UniProt *S. japonicum* database. For protein identification, parameters of 1) peptide mass tolerance=20 ppm; 2) MS/MS tolerance=0.1 Da; 3) Enzyme=Trypsin; 4) Missed cleavage=2; 5) Fixed modification: Carbamidomethyl (C), iTRAQ4/8plex (K), iTRAQ4/8plex (N-term); 6) Variable modification: Oxidation (M); 7) Phosphorylation (S/T/Y); 8) protein FDR<0.01.

Blast2GO was used to predict the biological processes of *S. japonicum* phosphoproteins [50]. String (http://string-db.org/) was used to predict protein-protein interaction and the results were visualized by Cytosacpe (3.6.1). The peptide FDR is lower than 1% for database searching in the present study. The DEPs were defined using DEqMS (R packages, a tool to perform statistical analysis of differential protein expression for quantitative proteomics data) [51], with a cutoff of adjusted $p<0.05$ and fold-change>1.5.

## Single-cell RNA sequencing analysis

Single-cell RNA (scRNA) sequencing data of *S. mansomi* by Wendt et al., was downloaded from NCBI Gene Expression Omnibus under accession number GSE146737. Seurat package (https://satijalab.org/seurat/), a widely adopted framework in bioinformatics was employed to analyze the scRNA data and the visualization, following the official analytical workflow. We adopted the cell type annotation in the published paper.

## Real-time qPCR (RT-qPCR)

Total RNAs were isolated from adult male and female schistosomes (35 dpi) using Trizol (Thermo Fisher Scientific ) following the manufacturer's instruction and real-time RT-PCR was performed. Briefly, total RNA was added to a reverse transcript transcription reaction containing multi-Scribe reverse transcriptase reagent and random hexamers (Eppendorf),

400 incubated at 25° C for 10 min, 48° C for 30 min, and 95° C for 5 min. RT-qPCR was performed using 1μl cDNA in a final
401 volume of 25 μl containing 12.5μl 2×One-Step TB Green PrimeScript RT-PCR Kit (Cat: RR066A, Takara), 10.5 μl $H_2O$, and
402 1μl (10 μM) specific primers for the corresponding proteins in Mastercycler ep realplex (Eppendorf) using following thermal
403 cycling profile: 95°C for 30 s, followed by 40 cycles of amplification (95° C for 5s, 62° C for 30s).
404
405 The primers of *nicotinamide adenine dinucleotide dehydrogenase* (*NADH*) (forward primer: CGA GGA CCT AAC AGC AGA
406 GG; reverse primer: TCC GAA CGA ACT TTG AAT CC) were used as an internal control for normalization. In the present
407 study, quantification of the transcript of target genes relative to *NADH* was calculated using the following equation $N = 2^{-\Delta Ct}$,
408 $\Delta Ct = Ct^{target} - Ct^{NADH}$[52].
409
410 dsRNA preparation and treatment for schistosomes
411 According to the manufacturer's instructions, long dsRNA was synthesized in vitro using PCR products with the T7
412 Megascript RNAi Kit (Cat: AM1333, Thermo Fisher Scientific). Briefly, all synthesis reactions were incubated at 37° C for
413 12 hrs, followed by DNase treatment. Finally, the recovered dsRNA products were run on a 1% agarose gel to check their
414 integrity. This study employed the incubation method for dsRNA delivery. The synthesized dsRNA described above was
415 added to the culture medium at a concentration of 30 μg/ml on day 1, day 2, and day 5. Finally, mRNA suppression levels
416 were measured via RT-qPCR at 6 days post-silencing.
417
418 RNA interference
419 Each dsRNA duplexes (3μg per shot) was electroporated (125 V, 20 ms, 1 pulse in 200μl RPMI 1640 media) into cultured
420 schistosomes (25 days). Then, the parasites were transferred into a 12-well cell culture plate containing 2 mL complete RPMI-
421 1640 media supplemented with 2 g/L glucose, 0.3 g/L L-glutamine, 2.0 g/L $NaHCO_3$, 15% fetal bovine serum (heat
422 inactivated), and 5% pen/strep (10,000 units penicillin and 10 mg/streptomycin in 0.9% NaCl). To address potential
423 electroporation-induced effects, all groups (both control and RNAi treatment worms) were subjected to electroporation. Worm
424 viability was rigorously assessed before motility analysis, and only intact, actively moving worms were selected for
425 quantitative measurements. At 48, 96, or 108 hrs of post-electroporation, the parasites were collected and the total RNA was
426 isolated for real-time RT-qPCR analysis.
427
428 Three siRNA duplexes targeting EWB00-001858 duplexes (siRNA-392, siRNA-211, siRNA-824), three siRNA duplexes
429 targeting EWB00-010322 (siRNA-265, siRNA-1612, siRNA-2465) and one negative control siRNA (Supplementary Table7)
430 were designed, chemically synthesized, annealed in Shanghai GenePharma (China).
431
432 FastBlue BB staining
433 For FastBlue BB staining, worms from both the interference group and the control group were collected. Parasites were fixed
434 in 4% formaldehyde at room temperature for 4 hrs, then washed with PBSTx with shaking for 10 min at room temperature.
435 1% FastBlue BB staining solution was freshly prepared and filtered through a 0.22 μm filter. After staining the insects for 3
436 min, they were washed three times with PBSTx, each wash lasting 5 min. Subsequently, they were washed with 80% ethanol
437 for 10 min, mounted on slides, and observed under an optical microscope to assess the staining results and photographed.
438
439 Worm motility
440 After electroporated with inhibitors, male and female worms (at 25 dpi) were cultured for 5 days *in vitro*. Morphologic
441 alterations and motility of worms (at least 10 worms/well) were daily monitored using an inverted microscope with a 2.5-5×
442 lens, and quantified using the scoring system by WHO-TDR [53].
443
444 Statistical analysis
445 GraphPad Prism 9 (Boston, USA) software was used for statistical analysis and visualization. Student's *t*-test or ANOVA were
446 employed for comparing the means of 2 or >2 groups, respectively. The difference with $p<0.05$ is considered statistical
447 significance.
448

## Ethics statement

All experiments involving mice were carried out based on the Guide for the Care and Use of Laboratory Animals of the Ministry of Science and Technology of the People's Republic of China. All efforts were made to minimize animal suffering. All animal procedures were approved by the Animal Management Committee and the Animal Care and Use Committee of the Shanghai Science and Technology Commission of the Shanghai municipal government for Tongji University (TJAA00822501).

## Data availability

The datasets generated in the current study will be available at the National Genomics Data Center, Beijing Institute of Genomics, Chinese Academy of Sciences / China National Center for Bioinformatics upon acceptance for publication, under the project PRJCA040825.

## Credit authorship contribution statement

Chuantao Fang: Conceptualization, Investigation, Software, Formal analysis, Visualization, Writing-original draft. Bikash Giri: Formal analysis, Investigation, Visualization, Writing-original draft. Guofeng Cheng: Conceptualization, Investigation, Writing-original draft, Writing-review & editing. All authors have read and approved the final manuscript.

## Competing interests

The authors have declared no competing interests.

## Acknowledgments

This study was supported by the National Natural Science Foundation of China (31472187) and Fundamental Research Funds for the Central Universities from Tongji University. The study was also sponsored by the Shanghai Tongji University Education Development Foundation.

## ORCID

0000-0002-5876-3882 (Chuantao Fang)
0000-0002-6337-796X (Bikash R. Giri)
0000-0001-5249-1065 (Guofeng Cheng)

## References

1. AA Da'dara, Faghiri Z, Krautz-Peterson G, Bhardwaj R, Skelly PJ. Schistosome Na,K-ATPase as a therapeutic target. *Trans R Soc Trop Med Hyg*, 2013; 107:74-82.
2. DG Colley, Bustinduy AL, Secor WE, King CH. Human schistosomiasis. *Lancet*, 2014; 383:2253-64.
3. Global, regional, and national life expectancy, all-cause mortality, and cause-specific mortality for 249 causes of death, 1980-2015: a systematic analysis for the Global Burden of Disease Study 2015. *Lancet*, 2016; 388:1459-1544.
4. SA Thétiot-Laurent, Boissier J, Robert A, Meunier B. Schistosomiasis chemotherapy. *Angew Chem Int Ed Engl*, 2013; 52:7936-56.
5. AG Ross, Olveda RM, Acosta L, Harn DA, Chy D, Li Y, et al. Road to the elimination of schistosomiasis from Asia: the journey is far from over. *Microbes Infect*, 2013; 15:858-65.
6. MJ Doenhoff, Kusel JR, Coles GC, Cioli D. Resistance of *Schistosoma mansoni* to praziquantel: is there a problem? *Trans R Soc Trop Med Hyg*, 2002; 96:465-9.
7. A Danso-Appiah, De Vlas SJ. Interpreting low praziquantel cure rates of *Schistosoma mansoni* infections in Senegal. *Trends Parasitol*, 2002; 18:125-9.
8. TJ Blanchard. Schistosomiasis. *Travel Med Infect Dis*, 2004; 2:5-11.
9. W Kunz. Schistosome male-female interaction: induction of germ-cell differentiation. *Trends Parasitol*, 2001; 17:227-31.
10. AJ Walker, Rinaldi G, Shakir EMN. Molecular interactions between male and female schistosomes - a role for remote communication? *Trends Parasitol*, 2025; 41:28-37.
11. H Zhong, Wu L, Ren Y, Qin F, Jin Y. Comparative proteomic profiles of *Schistosoma japonicum* male worms derived from

498 single-sex and bisexual infections. *Int J Parasitol*, 2022; 52:815-828.
499 12. M Ressurreicao, De Saram P, Kirk RS, Rollinson D, Emery AM, Page NM, et al. Protein kinase C and extracellular signal-
500 regulated kinase regulate movement, attachment, pairing and egg release in *Schistosoma mansoni. PLoS Negl Trop Dis*,
501 2014; 8:e2924.
502 13. G Cheng, Luo R, Hu C, Lin J, Bai Z, Zhang B, et al. TiO2-based phosphoproteomic analysis of schistosomes:
503 characterization of phosphorylated proteins in the different stages and sex of *Schistosoma japonicum. J Proteome Res*,
504 2013; 12:729-42.
505 14. E Kalopothakis, Rumjanek F, Evans WH. Protein and antigen phosphorylation in the tegument of Schistosoma mansoni.
506 *Mol Biochem Parasitol*, 1987; 26:39-45.
507 15. R Luo, Zhou C, Lin J, Yang D, Shi Y, Cheng G. Identification of in vivo protein phosphorylation sites in human pathogen
508 *Schistosoma japonicum* by a phosphoproteomic approach. *J Proteomics*, 2012; 75:868-77.
509 16. L Zhao, Lu Z, He X, Mughal MN, Fang R, Zhou Y, et al. Serine/threonine protein phosphatase 1 (PP1) controls growth
510 and reproduction in *Schistosoma japonicum. Faseb j*, 2018;fj201800725R.
511 17. G Wendt, Zhao L, Chen R, Liu C, O'Donoghue AJ, Caffrey CR, et al. A single-cell RNA-seq atlas of *Schistosoma manson*i
512 identifies a key regulator of blood feeding. *Science*, 2020; 369:1644-1649.
513 18. J Wang, Chen R, Collins JJ, 3rd. Systematically improved in vitro culture conditions reveal new insights into the
514 reproductive biology of the human parasite *Schistosoma manson*i. *PLoS Biol*, 2019; 17:e3000254.
515 19. R Ma, Li S, Li W, Yao L, Huang HD, Lee TY. KinasePhos 3.0: Redesign and Expansion of the Prediction on Kinase-
516 specific Phosphorylation Sites. *Genomics Proteomics Bioinformatics*, 2023; 21:228-241.
517 20. M Chen, Zhang W, Gou Y, Xu D, Wei Y, Liu D, et al. GPS 6.0: an updated server for prediction of kinase-specific
518 phosphorylation sites in proteins. *Nucleic Acids Res*, 2023; 51:W243-w250.
519 21. B Buchfink, Reuter K, Drost HG. Sensitive protein alignments at tree-of-life scale using DIAMOND. *Nat Methods*, 2021;
520 18:366-368.
521 22. M Cannon, Stevenson J, Stahl K, Basu R, Coffman A, Kiwala S, et al. DGIdb 5.0: rebuilding the drug-gene interaction
522 database for precision medicine and drug discovery platforms. *Nucleic Acids Res*, 2024; 52:D1227-D1235.
523 23. J Yuan, Dong X, Yap J, Hu J. The MAPK and AMPK signalings: interplay and implication in targeted cancer therapy. *J*
524 *Hematol Oncol*, 2020; 13:113.
525 24. C Falcicchia, Tozzi F, Arancio O, Watterson DM, Origlia N. Involvement of p38 MAPK in Synaptic Function and
526 Dysfunction. *Int J Mol Sci*, 2020; 21.
527 25. F Zeng, Yi C, Zhang W, Cheng S, Sun C, Luo F, et al. A new ferritin SjFer0 affecting the growth and development of
528 *Schistosoma japonicum. Parasit Vectors*, 2022; 15:177.
529 26. Z Xie, Zhao M, Yan C, Kong W, Lan F, Narengaowa, et al. Cathepsin B in programmed cell death machinery: mechanisms
530 of execution and regulatory pathways. *Cell Death Dis*, 2023; 14:255.
531 27. X Piao, Duan J, Jiang N, Liu S, Hou N, Chen Q. *Schistosoma japonicum* Tyrosine Hydroxylase is promising targets for
532 immunodiagnosis and immunoprotection of Schistosomiasis japonica. *PLoS Negl Trop Dis*, 2023; 17:e0011389.
533 28. B Pereira Moreira, Weber MHW, Haeberlein S, Mokosch AS, Spengler B, Grevelding CG, et al. Drug Repurposing and De
534 Novo Drug Discovery of Protein Kinase Inhibitors as New Drugs against Schistosomiasis. *Molecules*, 2022; 27.
535 29. S Hahnel, Parker-Manuel R, Dissous C, Cailliau K, Grevelding CG. First characterization of SmOPG1, a novel protein
536 involved in gonad-associated processes in *Schistosoma mansoni. Mol Biochem Parasitol*, 2017; 213:22-25.
537 30. C Buro, Burmeister C, Quack T, Grevelding CG. Identification and first characterization of SmEps8, a potential interaction
538 partner of SmTK3 and SER transcribed in the gonads of *Schistosoma mansoni. Exp Parasitol*, 2017; 180:55-63.
539 31. M Ressurreição, Elbeyioglu F, Kirk RS, Rollinson D, Emery AM, Page NM, et al. Molecular characterization of host-
540 parasite cell signalling in *Schistosoma mansoni* during early development. *Sci Rep*, 2016; 6:35614.
541 32. C Thawornkuno, Srisuksai K, Simanon N, Adisakwattana P, Ampawong S, Boonyuen U, et al. A reanalysis and integration
542 of transcriptomics and proteomics datasets unveil novel drug targets for Mekong schistosomiasis. *Sci Rep*, 2024; 14:12969.
543 33. B Balikagala, Sakurai-Yatsushiro M, Tachibana SI, Ikeda M, Yamauchi M, Katuro OT, et al. Recovery and stable
544 persistence of chloroquine sensitivity in Plasmodium falciparum parasites after its discontinued use in Northern Uganda.
545 *Malar J*, 2020; 19:76.
546 34. H Wen, Yin L, Wang J, Zhang L, Sun T, Xu F, et al. Population pharmacokinetics and model-informed precision dosing of

547 lamivudine in Chinese HIV-infected patients with mild and moderate impaired renal function. *Expert Rev Clin Pharmacol*,
548 2022; 15:647-655.
549 35. ER Schiff. Lamivudine for hepatitis B in clinical practice. *J Med Virol*, 2000; 61:386-91.
550 36. NC Gomes-da-Silva, de Faria Almeida A, Severino P, Al-Qahtani M, Rebelo Alencar LM, Fechine PBA, et al. Exploring
551 the Anticancer Potential of Lamivudine-Loaded Polymeric Nanoparticles: In Vitro Cytotoxicity, Tissue Deposition,
552 Biochemical Impact In Vivo, and Molecular Simulations Analysis. *ACS Appl Bio Mater*, 2025.
553 37. MJ Buskes, Clements M, Bachovchin KA, Jalani HB, Leonard A, Bag S, et al. Structure-Bioactivity Relationships of
554 Lapatinib Derived Analogs against *Schistosoma mansoni*. *ACS Med Chem Lett*, 2020; 11:258-265.
555 38. F Ghaffarifar. Leishmania major: in vitro and in vivo anti-leishmanial effect of cantharidin. *Exp Parasitol*, 2010; 126:126-
556 9.
557 39. E Eldeeb, Fahmy S, Elbakry K, Hyder A. A single dose of the antineoplastics hydroxyurea or cisplatin has praziquantel-
558 like effects on *Schistosoma mansoni* worms and host mouse liver. *Biomed Pharmacother*, 2018; 99:570-575.
559 40. WC Van Voorhis, Doggett JS, Parsons M, Hulverson MA, Choi R, Arnold SLM, et al. Extended-spectrum antiprotozoal
560 bumped kinase inhibitors: A review. *Exp Parasitol*, 2017; 180:71-83.
561 41. A Bhattacharjee, Bagchi A, Sarkar S, Bawali S, Bhattacharya A, Biswas A. Repurposing approved protein kinase inhibitors
562 as potent anti-leishmanials targeting Leishmania MAP kinases. *Life Sci*, 2024; 351:122844.
563 42. KSP Mogwera, Chibale K, Arendse LB. Developing kinase inhibitors for malaria: an opportunity or liability? *Trends*
564 *Parasitol*, 2023; 39:720-731.
565 43. LB Arendse, Wyllie S, Chibale K, Gilbert IH. Plasmodium Kinases as Potential Drug Targets for Malaria: Challenges and
566 Opportunities. *ACS Infect Dis*, 2021; 7:518-534.
567 44. JR Wisniewski, Zougman A, Nagaraj N, Mann M. Universal sample preparation method for proteome analysis. *Nat*
568 *Methods*, 2009; 6:359-62.
569 45. MR Larsen, Thingholm TE, Jensen ON, Roepstorff P, Jorgensen TJ. Highly selective enrichment of phosphorylated
570 peptides from peptide mixtures using titanium dioxide microcolumns. *Mol Cell Proteomics*, 2005; 4:873-86.
571 46. N Colaert, Van Huele C, Degroeve S, Staes A, Vandekerckhove J, Gevaert K, et al. Combining quantitative proteomics
572 data processing workflows for greater sensitivity. *Nat Methods*, 2011; 8:481-3.
573 47. S Lemeer, Kunold E, Klaeger S, Raabe M, Towers MW, Claudes E, et al. Phosphorylation site localization in peptides by
574 MALDI MS/MS and the Mascot Delta Score. *Anal Bioanal Chem*, 2012; 402:249-60.
575 48. PL Ross, Huang YN, Marchese JN, Williamson B, Parker K, Hattan S, et al. Multiplexed protein quantitation in
576 Saccharomyces cerevisiae using amine-reactive isobaric tagging reagents. *Mol Cell Proteomics*, 2004; 3:1154-69.
577 49. SA Beausoleil, Villen J, Gerber SA, Rush J, Gygi SP. A probability-based approach for high-throughput protein
578 phosphorylation analysis and site localization. *Nat Biotechnol*, 2006; 24:1285-92.
579 50. A Conesa, Götz S, García-Gómez JM, Terol J, Talón M, Robles M. Blast2GO: a universal tool for annotation, visualization
580 and analysis in functional genomics research. *Bioinformatics*, 2005; 21:3674-6.
581 51. Y Zhu, Orre LM, Zhou Tran Y, Mermelekas G, Johansson HJ, Malyutina A, et al. DEqMS: A Method for Accurate Variance
582 Estimation in Differential Protein Expression Analysis. *Mol Cell Proteomics*, 2020; 19:1047-1057.
583 52. KJ Livak, Schmittgen TD. Analysis of relative gene expression data using real-time quantitative PCR and the 2(-Delta
584 Delta C(T)) Method. *Methods*, 2001; 25:402-8.
585 53. S Townson, Ramirez B, Fakorede F, Mouries MA, Nwaka S. Challenges in drug discovery for novel antifilarials. *Expert*
586 *Opin Drug Discov*, 2007; 2:S63-73.
587
588

589 **Figure legends**

590

591 **Fig.1 Overview of iBQP and iBQPP protein profiles**

592 A. Workflow (including animal model construct, worm collection/separation, protein sample preparation, LC-MS/MS, and
593 bioinformatics) of the current study. dpi, days post-infection; iTRAQ, Isobaric Tags for Relative and Absolute
594 Quantitation.

595 B. Distribution of unique peptide coverage (Top) and total peptide (Bottom) of 2,055 proteins identified. Proteins with a
596 high coverage ratio (>50%, in a dashed line rectangle) were subjected to functional enrichment analysis in E).

597 C. Venn plot indicated the relationship between the proteomic data with 3 widely used protein annotations of *S. japonicum*.
598 AH, Anhui version of PRJEA34885 (https://parasite.wormbase.org/Schistosoma_japonicum_prjea34885/Info/Index/);
599 FD, Fudan version of PRJNA520774 (https://parasite.wormbase.org/Schistosoma_japonicum_prjna520774/Info/Index/);
600 and UniProt, retrieved by the keyword of taxonomy_id:6182.

601 D. Overview of protein-coding gene (identified by proteomics and phosproteomics) locus on 9 chromosomes of *S. japonicum*.
602 The chromosomes were defined by the Genome assembly ASM2521551v1 of *S. japonicum*.

603 E. Functional enrichment analysis of high expressed proteins in proteomics using Gene Ontology (GO) gene sets. BP
604 (biological processes) and CC (cellular component) are defined by the GO database. The top 20 enriched terms were
605 presented.

606

607 **Fig.2 Differentially expressed proteins between male and female worms**

608 A. Heatmap showing differentially expressed proteins between male and female worms in three biological replicates. The
609 cutoff of fold-change >1.5 and adjusted $p<0.05$ was used as the cutoff. exp, expression.

610 B. The overlap between differentially expressed genes (in RNA-seq) and proteins (in proteomics of the current study). Both
611 are differentially expressed in protein and mRNA levels; Protein/RNA is only differentially expressed in protein/mRNA
612 levels.

613 C. Functional enrichment analysis using gene sets defined by the Gene Ontology and KEGG. BP, biological processes; CC,
614 cellular components; MF, molecular function. $P<0.05$ was used as a cutoff. The top 10 enriched terms were presented.
615 NES, normalized Enrichment, Score.

616 D. Protein-protein interaction of identified differentially expressed proteins. STRINGdb R package was employed for the
617 analysis.

618 E. Annotation of selected proteins in cell clusters from single-cell RNA seq dataset. *Catb1* and *Ft* expression in two-
619 dimension Uniform Manifold Approximation and Projection (UMAP) space of *S. mansoni* single-cell RNA sequencing
620 data by Wendt et al., 2020 [17]. Exp, expression in single-cell RNA dataset.

621 F. FastBlue BB analysis of morphological vitellarium in *Catb1* or *Ft* inhibited females. Worms targeted the *Catb1* and *Ft*
622 via RNAi were used. n=10, scale bar, 100μm. RNAi, RNA interference.

623 G. Egg count of the females treated with *Catb1* or *Ft* dsRNA. The same worms in F) were used. $*P<0.05$ was calculated by
624 one-way ANOVA with multiple comparison test.

625 H. Effect of *Mcm4* or *Agp* inhibition on worm mobility. $**p<0.01$ and $***p<0.001$ and ns, no significance by one-way
626 ANOVA with multiple comparison test.

627 I. Egg count of the females treated with *Mcm4* or *Agp* siRNA.$*p<0.01$ and $**p<0.001$ by one-way ANOVA with multiple
628 comparison test.

629

**Fig.3 Differentially expressed phosphorylated proteins between male and female worms.**

A. Venn plot indicated the relationship between the proteomic data with 3 widely used protein annotations of *S. japonicum* and the mentioned proteome data. AH, Anhui version of PRJEA34885 (https://parasite.wormbase.org/Schistosoma_japonicum_prjea34885/Info/Index/); FD, Fudan version of PRJNA520774 (https://parasite.wormbase.org/Schistosoma_japonicum_prjna520774/Info/Index/); and Uniprot, retrieved by the keyword of taxonomy_id:6182.

B. Distribution of the number of peptide-modified sites with the indicated probability.

C. The number of peptide S/T modifications.

D. Principal component analysis of phosphoproteomic data.

E. Heatmap showing differentially expressed phosphorylated proteins between male and female worms in three biological replicates. The cutoff of fold-change>1.5 and adjusted $p<0.05$ was used.

F. The recall proportion of identified phosphorylation sites by KinasePhos software, kinase-specific phosphorylation site prediction tools (https://awi.cuhk.edu.cn/KinasePhos/About%20KinasePhos.html). Probability, the probability of being a real modification.

G. Functional enrichment of high probable phosphorylated proteins by gene ontology-defined gene sets. The top 10 enriched terms were presented.

H. The total number of predicted phosphorylation sites (with probability>0.5) of the indicated kinases. Kinases of S/T/ST modification were predicated by GPS6.0.

**Fig.4 Differentially expressed kinases between males and females**

A. Flowchart for predicting *S. japonicum* kinases and their interactors. *S. japonicum* kinases were predicted based on a protein sequence homology (identity>30%) with *C. elegans* kinases (423). Kinase substrate gene sets were defined by STRING online tools.

B. Heatmap of kinase activity calculated by GSVA algorithm. Kinase activity was defined by the enrichment score of kinase substrates in A).

C. Principal component analysis of kinase activity of female and male worms.

D. Volcano plot showing the different kinase activities between male and female worms.

E. GO enrichment analysis of kinases with different activity between female and male worms. The top 10 enriched terms were presented.

661

**Table 1. Female enriched phosphorylated proteins in *S. japonicum***

| # | Protein IDs | Protein names | Phosphopeptide sequences |
|---|---|---|---|
| 1 | CPRT0000000621<br>Sjc_0006630 | Serine beta-lactamase-like protein LACTB | vLPcQPsEEsDVEDYIETSDk |
| 2 | AAX27515.2 | SJCHGC07767 | vEVtGTPR |
| 3 | AAX27427.2 | SJCHGC09055 protein | qTSANDssDEEIDNQLk |
| 4 | CPRT0000000458<br>Sjc_0004860 | Protein transport protein SEC31 | vAEAFDDEQPLINFSNEHNNNNIsPISSLR |
| 5 | AAW26505.1 | SJCHGC02563 protein | sVSNFELENNR<br>vRsVsNFELENNR<br>vRsVSNFELENNR<br>sVsNFELENNR<br>sQGtLGNNSIYSDR |
| 6 | CPRT0000001874<br>Sjc_0020010 | Ryanodine receptor 3 | rQtItSDNLLNYNPSPk |
| 7 | CPRT0000004808<br>Sjc_0051030 | oxidative-stress responsive 1 | aSGGSVGVDsDDDsDENDYk<br>nNsTEWNFDTVGR<br>aSGGsVGVDsDDDsDENDYk<br>aSGGSVGVDSDDDsDENDYk |
| 8 | AAK54601.1 | Y-box DNA-binding protein | dNYHNEDGsPDMRDA<br>dNYHNEDGsPDMR<br>dNYHNEDGsPDmR<br>dNYHNEDGsPDmRDA |
| 9 | CPRT0000006683<br>Sjc_0071060 | Ribonucleoside-diphosphate reductase beta chain | gEPTHNFsIDEDF |
| 10 | CPRT0000003382<br>Sjc_0035830 | Conserved hypothetical protein | gVQDLDsHVGsLTTLAR<br>gVQDLDSHVGsLTTLAR<br>gVQDLDSHVGsLttLAR<br>sYQGsESDLAYk<br>eMSSsSSR<br>aHSttPTR |
| 11 | CPRT0000004524<br>Sjc_0048020 | | nkEEIEIDEDsD |
| 12 | AAP06137.1 | Similar to NM_078233 ZK1073 | sLsMEEYDQPk<br>lHDEsPINEYDDHNIA |
| 13 | CPRT0000003363<br>Sjc_0035630 | Phosphorylase kinase | sPSHVVSSEQItPINsPsYSGTHSR<br>sPSHVVSSEQItPINsPSYSGTHSR<br>kQsIVsTEVENENSHADSR<br>rTSDGRssGcGLDSTDWLNSLSPDQLVk |
| 14 | CPRT0000005708<br>Sjc_0060630 | MYM-type zinc finger protein 2 | aVEsEDDDDDDDMVPVGEIDDDQPLLTk<br>aVEsEDDDDDDDmVPVGEIDDDQPLLTk |
| 15 | CPRT0000004379<br>Sjc_0046520 | Conserved hypothetical protein | gEMsLsPEMR<br>gEMSLsPEMR<br>gVDSGWDSDMLsSDGVR<br>gEMsLsPEmR<br>gEMSLsPEmR<br>gVDSGWDSDMLssDGVR |

| | | | |
|---|---|---|---|
| 16 | AAW27184.1 | Similar to von Hippel-Lindau binding protein 1 | qNQSsGANA |
| 17 | CPRT0000004159<br>Sjc_0044150 | Similar to Lon protease homolog | hLHHTGDSFsDtDSSDEASHk<br>hLHHTGDSFsDtDsSDEASHk |
| 18 | CAX69334.1 | Cysteine-rich protein 1 | gYGAVPNSENFs |
| 19 | CPRT0000000881<br>Sjc_0009420 | Microtubule-associated protein 7 | aPsNQsSNASLSIEER<br>tAsAsPSLGMSR<br>tAsAsPSLGmSR<br>aPsNQssNASLSIEER<br>vTFTIDGEQENESSssLEEsVSQSPLSk |
| 20 | CPRT0000004177<br>Sjc_0044380 | Tensin | tVTPFsPtGSLSGTNIGTDVVDGDTAGMR<br>qNsQYEATPLVANR<br>qNsQyEATPLVANR<br>tVTPFsPtGSLSGTNIGTDVVDGDTAGmR<br>tVTPFSPTGSLSGtNIGTDVVDGDTAGMR<br>tVTPFsPtGsLSGTNIGTDVVDGDTAGMR<br>tVTPFsPtGsLSGTNIGTDVVDGDTAGmR<br>vPPNsPR |
| 21 | CPRT0000001808<br>Sjc_0019300 | Cell division control related protein 1 | lPEcDsDEEDEIkR<br>lPEcDsDEEDEIk<br>iDIYRLPEcDsDEEDEIk |
| 22 | CPRT0000005421<br>Sjc_0057570 | Fermitin-1 | lQLDDNtSR |
| 23 | CPRT0000009689<br>Sjc_0102960 | Actin dependent regulator of chromatin | lDDSSFMDDGssETGSVIMAAPQAAk<br>aIDEGsLEEAEER |
| 24 | CAX83117.1 | Eukaryotic translation initiation factor 3 subunit | iESRPLHLssDEEDIkR |
| 25 | AAW26926.1 | SJCHGC05742 protein | yVEAtSGILNV |
| 26 | CPRT0000008329<br>Sjc_0088510 | Ran-binding protein 2 | eIVDLDQNGDDtDsDVVVVELPLQVSDDQLSR<br>sNADTTAEQsDSDSTVk<br>sNADTTAEQsDsDSTVk |
| 27 | AAX30178.1 | Transcriptional Coactivator p15 | aEssDssLsDLEEPIEVk |

662

663

664
665

**Table 2. Male enriched phosphorylated proteins in *S. japonicum***

| # | Protein IDs | Protein names | Phosphopeptide sequences |
|---|---|---|---|
| 1 | CPRT0000004711 | Dynamin-1 | aEQSDNSsLDASEPQLER |
| 2 | CPRT0000008652<br>Sjc_0091980 | Tubulin alpha-1 chain | eDLAALEkDYEEVASDTVDAQsDDGF<br>dYEEVASDTVDAQsDDGF<br>eDLAALEkDYEEVAsDTVDAQsDDGF |
| 3 | AAW26889.1 | SJCHGC06753 protein | tFYFDVGSNR |
| 4 | AAW26211.1 | SJCHGC02263 protein | kSNYELTHVNGDAsPAsIR |
| 5 | CPRT0000007806<br>Sjc_0082920 | MCM3 minichromosome maintenance deficient 3 | dRNEDDGVNEsDNEsENGDDTER |
| 6 | CPRT0000000573<br>Sjc_0006120 | Kismet | sAFYGDDsGsEPDVSSR |
| 7 | CPRT0000008409<br>Sjc_0089390 | Synapsin-3 | rFsSGDLQGELADk<br>gAYPsAPTsPTR<br>gAYPSAPTsPTR |
| 8 | CPRT0000008394<br>Sjc_0089220 | FKBP-rapamycin associated protein | vFTNPDHPDsVsLRDPQk |
| 9 | CPRT0000007233<br>Sjc_0076870 | SWI/SNF-related matrix-associated actin-dependent regulator of chromatin subfamily C member 2 | rRsPsPSASDSTLPPNAGGk<br>rsPSPsASDSTLPPNAGGk<br>sPsPSASDSTLPPNAGGk |
| 10 | CPRT0000004252<br>Sjc_0045180 | E3 ubiquitin-protein ligase HUWE1 | sSAPQNLPsPSDQTk |
| 11 | AAW25135.1 | SJCHGC06536 protein | rAAIDsDEDsL<br>aAIDsDEDsL<br>aAIDSDEDsL |
| 12 | AAX27232.2 | Rat1 Kar1/Rat1 like 5'-3' exonuclease | kLNSDENATGsS<br>lNSDENATGsS |
| 13 | CAX69585.1 | Microtubule-associated protein futsch | sNkPTDTSsPPASLFDFESFLcDMMSk<br>sAsNEssINsVEQNHNTSR<br>sAsNEssINSVEQNHNTSR<br>sAsNEsSINSVEQNHNTSR<br>sAsNESSINSVEQNHNTSR |
| 14 | AAX28334.2 | Cytoplasmic dynein 1 intermediate chain 2 | eLEsPSHDVNDSILQR |
| 15 | AAW26234.1 | Aldolase_II | aNsDSGDIPWTPAELEFEAEMR<br>aNsDsGDIPWTPAELEFEAEMR<br>aNsDSGDIPWTPAELEFEAEmR<br>rstDFNR |
| 16 | CAX78355.1 | Nascent polypeptide-associated complex subunit alpha | vAsDsDsDsDDsAPELENSk<br>vAsDsDsDsDDSAPELENSk |
| 17 | CPRT0000002334<br>Sjc_0024830 | Ndr, domain-containing protein | lSQQVPEENtT<br>qksPELsPEER |
| 18 | AAW26348.1 | Ribosomal protein L22 | fFNFENEDtDDEEES |
| 19 | CAX70261.1 | nervana 2 | sMQEFsDNLsTLsYMsR |
| 20 | AAW27478.1 | Alpha tubulin | eDLAALEkDYEEVGVDsVDGEGEGEGEEY<br>tIGGGDDsFNTFFSETGAGk |
| 21 | CPRT0000008703<br>Sjc_0092520 | Twinstar | gDLQADDISEVtESALASk |

| | | | |
|---|---|---|---|
| 22 | CAX69776.1 | Transmembrane protein 66 precursor | rNPsAPPsPEYGWSSNVMGSSQSR<br>rsRtPsPETHISSGFGGTSR<br>sRtPsPETHISSGFGGTSR |
| 23 | CAX71152.1 | Actin 5C | lcYVALDFEQEMATAASSsSLEk |
| 24 | AAP06094.1 | Hypothetical protein | rSsNTNSEEsPVTR<br>iAAAQAAsPAksPAksPR<br>aASEDTEsQQsQVk<br>iAAAQAASPAksPAksPR<br>sSNTNSEEsPVTR<br>rsSNTNSEESPVTR<br>iAAAQAAsPAksPAk<br>aASEDtESQQSQVk |
| 25 | CPRT0000003978<br>Sjc_0042230 | FERM domain-containing protein 5 | iYLPISTGATGNSsPSTNVk<br>lRPSDDSsGDR<br>acTGsIANLPQQsFSR<br>acTGSIANLPQQSFsR<br>lRPSDDssGDRSERPR |
| 26 | CAX73031.1 | Epidermal growth factor receptor pathway substrate 8 | sAEIQLPPMVTkEDsVYsESQINR<br>eDSVYsESQINR<br>eDsVYsESQINR<br>sAEIQLPPMVTkEDsVYSESQINR<br>yVNLGDsTFGMNRsPk<br>sAEIQLPPmVTkEDsVySESQINR |
| 27 | CPRT0000008093<br>Sjc_0085990 | Nuclear pore complex protein Nup98 | lDDsDEGEGDDcDsDSLSk<br>yRLDDsDEGEGDDcDsDSLSk<br>lDDsDEGEGDDcDSDSLSk |
| 28 | CPRT0000012522<br>Sjc_0085870 | DNA-directed RNA polymerase | tWLQLtPFITNASScEcIEDLFR |
| 29 | CPRT0000008868<br>Sjc_0094310 | Skeletal muscle LIM-protein 3 | gFLTSDDMIMcsDcGR |
| 30 | AAW26770.1 | Hypothetical protein | qLsPEYPcITIYYSDMDSELENk |
| 31 | CPRT0000000900<br>Sjc_0009630 | Plasma membrane calcium ATPase 3 isoform 3a | ssLGsGDANTTEDSSDAPk<br>sSLGsGDANttEDSSDAPk |
| 32 | CAX73986.1 | Myeloid/lymphoid or mixed-lineage leukemia 2 | rGssGsPFASHSTDRPR<br>rPsPPGNR |
| 33 | CPRT0000006393<br>Sjc_0068000 | ATP-binding cassette, sub-family F, member 1 | aITAVsLDDEVGNFISR |
| 34 | AAW24493.1 | SJCHGC09143 protein | hVsEsEDDER<br>hVsEsEDDERR<br>hVsESEDDER |
| 35 | CPRT0000005368<br>Sjc_0056980 | GlcNAc-1-P transferase | tENVAPQAGHENmssDEEQISER<br>tENVAPQAGHENMssDEEQISER<br>tENVAPQAGHENMSsDEEQISER<br>tENVAPQAGHENmsSDEEQISER |
| 36 | CPRT0000002258<br>Sjc_0024050 | Alpha-adducin | lAPPPTTGTLTsEPsGTEDMSESDGk |
| 37 | AAW27426.1 | SJCHGC02665 protein | kLAILIDPSLVIDEPVQNsDssHDsDTTSIR<br>lAILIDPsLVIDEPVQNsDSSHDSDTTSIR |

| | | | |
|---|---|---|---|
| | | | lAILIDPsLVIDEPVQNsDsSHDSDTTSIR |
| 38 | CPRT0000003639<br>Sjc_0038600 | Myelin expression factor 2 | yEDSEsPDIPSR<br>sIkYEDsEsPDIPSR<br>hRsPIDRGsR<br>sIkYEDSEsPDIPSR |

666

**Table 3 *S. japonicum* kinases that share homology with human kinase targeted by FDA-approved drugs**

| UniProt | Symbol | Identity[a] | *P*[b] | Drug | Concept[c] | Score[d] | FDA |
|---|---|---|---|---|---|---|---|
| A0A4Z2DKT9 | AKT3 | 63.1 | 7.82E-150 | Capivasertib | rxcui:2669967 | 0.469 | Yes |
| A0A4Z2DI92 | BRSK1 | 63.2 | 6.17E-166 | Gefitinib | rxcui:328134 | 0.041 | Yes |
| A0A4Z2DY93 | CDK12 | 67.5 | 2.11E-160 | Enzalutamide | rxcui:1307298 | 0.808 | Yes |
| A0A4Z2DU38 | CDK19 | 71.2 | 4.86E-194 | Pexidartinib | rxcui:2183102 | 0.25 | Yes |
| C1L6Q8 | CDK5 | 77.9 | 1.67E-167 | Palbociclib | rxcui:1601374 | 0.024 | Yes |
| A0A4Z2DBA4 | CSNK1A1 | 64.9 | 1.68E-151 | Heparin | rxcui:5224 | 0.205 | Yes |
| A0A4Z2CN04 | CSNK1E | 80.8 | 3.26E-179 | Umbralisib tosylate | rxcui:2478438 | 4.376 | Yes |
| C1L7H2 | CSNK2A3 | 81.7 | 1.2E-207 | Cisplatin | rxcui:2555 | 0.724 | Yes |
| A0A4Z2D4C4 | CTDSP1 | 61.9 | 9.91E-77 | Isopropamide iodide | rxcui:6051 | 0.691 | Yes |
| A0A4Z2D4C4 | CTDSP1 | 61.9 | 9.91E-77 | Cefuroxime sodium | rxcui:204144 | 0.691 | Yes |
| A0A4Z2D4C4 | CTDSP1 | 61.9 | 9.91E-77 | Cefdinir | rxcui:25037 | 0.691 | Yes |
| A0A4Z2D9D4 | DYRK1A | 62.1 | 1.29E-129 | Belumosudil | rxcui:2564025 | 0.239 | Yes |
| A0A4Z2CZB0 | EEF2K | 64.7 | 4.83E-108 | Lapatinib | rxcui:480167 | 1.694 | Yes |
| Q5DB16 | GNB3 | 77.9 | 1.55E-153 | Sildenafil | rxcui:136411 | 0.796 | Yes |
| Q5DB16 | GNB3 | 77.9 | 1.55E-153 | Telmisartan | rxcui:73494 | 0.796 | Yes |
| A0A4Z2CT59 | GRK2 | 71.1 | 8.18E-114 | Chloroquine | rxcui:2393 | 0.547 | Yes |
| A0A4Z2D605 | GSK3A | 75.9 | 7.1E-183 | Lithium citrate | rxcui:52105 | 0.673 | Yes |
| Q6PMM5 | MAPK3 | 67.7 | 1.3E-174 | Nitroglycerin | rxcui:4917 | 0.152 | Yes |
| Q5D9F6 | MAPK8 | 69.9 | 2.06E-181 | Dexrazoxane | rxcui:42736 | 0.412 | Yes |
| A0A4Z2D1I5 | MARK2 | 78.8 | 5.47E-180 | Acetaminophen | rxcui:161 | 0.096 | Yes |
| A0A4Z2CQ40 | PAK4 | 61.3 | 1.12E-112 | Palbociclib | rxcui:1601374 | 0.045 | Yes |
| Q7Z0T1 | PGK1 | 69.3 | 1.92E-205 | Lamivudine | rxcui:68244 | 2.188 | Yes |
| C7TYW7 | PICK1 | 66 | 1.14E-179 | Methamphetamine | rxcui:6816 | 4.376 | Yes |
| Q5DAM7 | PKLR | 62.5 | 3.89E-215 | Mitapivat sulfate | rxcui:2595574 | 17.503 | Yes |
| Q5DAL5 | PPP1CA | 85.7 | 2.3E-217 | Cantharidin | rxcui:1984 | 5.251 | Yes |
| A0A4Z2D915 | PPP3CB | 73.7 | 1.08E-264 | Voclosporin | rxcui:2475166 | 8.751 | Yes |
| A0A4Z2DRM5 | PRKCB | 65 | 1.58E-238 | Dexmedetomidine hydrochloride | rxcui:228054 | 0.597 | Yes |
| A0A4Z2DSA0 | PTPRS | 68.3 | 1.92E-276 | Etidronic acid | rxcui:1356715 | 3.751 | Yes |
| C1LDQ2 | STK4 | 68 | 9.87E-134 | Bosutinib | rxcui:1307619 | 0.326 | Yes |
| C1L3R1 | SYT2 | 72.9 | 2.05E-145 | Botulinum toxin type b | rxcui:2167673 | 35.005 | Yes |
| A0A4Z2CY17 | TLE3 | 62.8 | 1.36E-144 | Docetaxel anhydrous | rxcui:1299922 | 0.316 | Yes |

[a] The identity of *S japonicum* and human proteins is defined by Diamond software, a well-known protein sequence alignment tool.

[b] *P* for the identity of *S. japonicum* and human proteins defined by Diamond software.

[c] Drug concept identifier defined by RxNorm, a database providing normalized names for clinical drugs and links its names to many of the drug vocabularies commonly used in pharmacy management and drug interaction software.

[d] Score, evidence score defined by DGIdb (https://www.dgidb.org/about#interaction-scores).

667

668 **Supplementary material**

669 **Fig.S1 Overview of iBQP and iBQPP protein profiles**

670 A. Functional enrichment analysis of highly expressed proteins in proteomics using GO and KEGG gene sets. MF, molecular
671 function of GO database; KEGG, Kyoto Encyclopedia of Genes and Genomes. The top 20 enriched terms were presented.

672

673 **Fig.S2 Differentially expressed proteins between male and female worms**

674 A. Principal component analysis of proteomic data.

675 B. Boxplot showed the total count of peptides among the samples.

676 C. The correlation of mRNAs (by RNA seq) and proteins (by proteomic) abundance of *S. japonicum.* The mRNA levels
677 were quantified using TPM (Transcripts Per Kilobase of exon model per Million mapped reads), and the protein levels
678 were defined by the normalized peptide count using peptide length.

679 D. Heatmap of differentially expressed genes between male and female worms. The cutoff of fold-change>1.5 and $p<0.05$
680 was used.

681 E. Volcano plot showing the differentially expressed genes/proteins between male and female worms.

682 F. Real-time PCR analysis of the knockdown efficiency of siRNA targeting the indicated protein-coding genes. Independent
683 siRNA targeting different sites was designed. $^{**}p<0.01$, and $^{***}p<0.001$.

684

685 **Fig.S3 Differentially expressed kinases between male and female**

686 A. Boxplot showed the total count of phosphorylated peptides among samples.

687 B. Distribution of unique peptide coverage/total peptide of 1,833 phosphorylated proteins identified.

688 C. The distribution of peptides on full-length protein (Top) and peptide length (Bottom).

689 D. The motif of specific kinases by the Motifx software.

690

691 **Fig.S4 Specific kinase motif by MEME**

692 The motifs of the indicated kinases are predicted by MEME software. Default settings were used in the analysis.

693

694 **Supplementary tables:**

695 Supplementary Table 1 The basic information of iTRAQ-based quantitative proteome (iBQP)

696 Supplementary Table 2 Expression matrix of iBQP

697 Supplementary Table 3 Differentially expressed proteins of iBQP

698 Supplementary Table 4 Differentially expressed genes between males and females from the public RNA-seq dataset of *S.*
699 *japonicum* (PRJNA428455)

700 Supplementary Table 5 The basic information of iTRAQ-based quantitative phosphoproteome

701 Supplementary Table 6 Differentially expressed phosphorylated proteins of iBQP.

702 Supplementary Table 7 siRNA sequence for targeting the indicated genes

703 Supplementary Table 8 The list of drugs for potentially targeting *S. japonicum* kinases
704

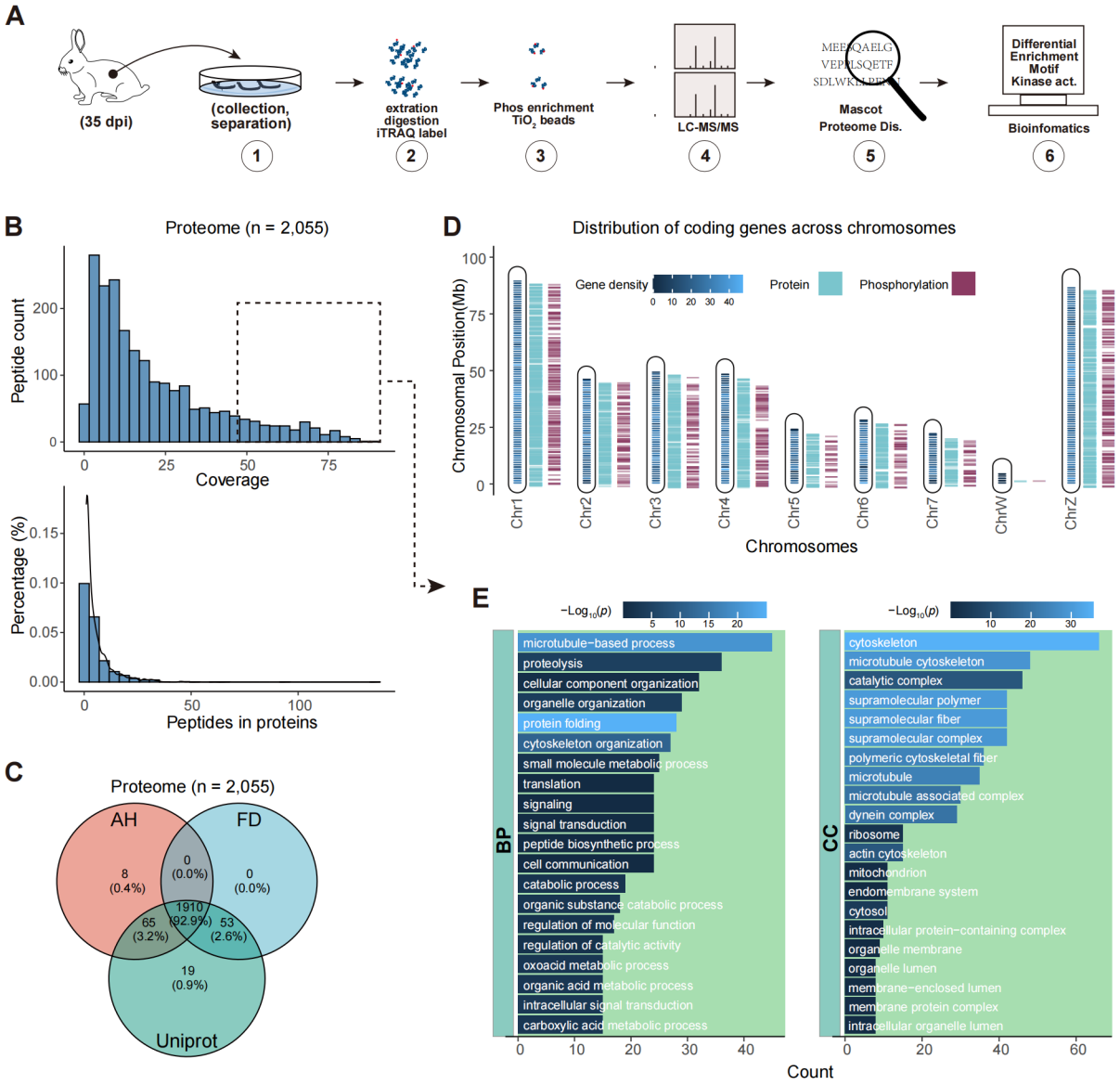
A
(35 dpi)
(collection, separation)
1
extration digestion iTRAQ label
2
Phos enrichment TiO2 beads
3
LC-MS/MS
4
Mascot Proteome Dis.
5
Differential Enrichment Motif Kinase act.
Bioinfomatics
6
B
Proteome (n = 2,055)
Peptide count
Coverage
Percentage (%)
Peptides in proteins
C
Proteome (n = 2,055)
AH
FD
Uniprot
8 (0.4%)
0 (0.0%)
0 (0.0%)
1910 (92.9%)
65 (3.2%)
53 (2.6%)
19 (0.9%)
D
Distribution of coding genes across chromosomes
Chromosomal Position(Mb)
Gene density
Protein
Phosphorylation
Chr1
Chr2
Chr3
Chr4
Chr5
Chr6
Chr7
ChrW
ChrZ
Chromosomes
E
−Log10(p)
BP
microtubule−based process
proteolysis
cellular component organization
organelle organization
protein folding
cytoskeleton organization
small molecule metabolic process
translation
signaling
signal transduction
peptide biosynthetic process
cell communication
catabolic process
organic substance catabolic process
regulation of molecular function
regulation of catalytic activity
oxoacid metabolic process
organic acid metabolic process
intracellular signal transduction
carboxylic acid metabolic process
CC
cytoskeleton
microtubule cytoskeleton
catalytic complex
supramolecular polymer
supramolecular fiber
supramolecular complex
polymeric cytoskeletal fiber
microtubule
microtubule associated complex
dynein complex
ribosome
actin cytoskeleton
mitochondrion
endomembrane system
cytosol
intracellular protein−containing complex
organelle membrane
organelle lumen
membrane−enclosed lumen
membrane protein complex
intracellular organelle lumen
Count

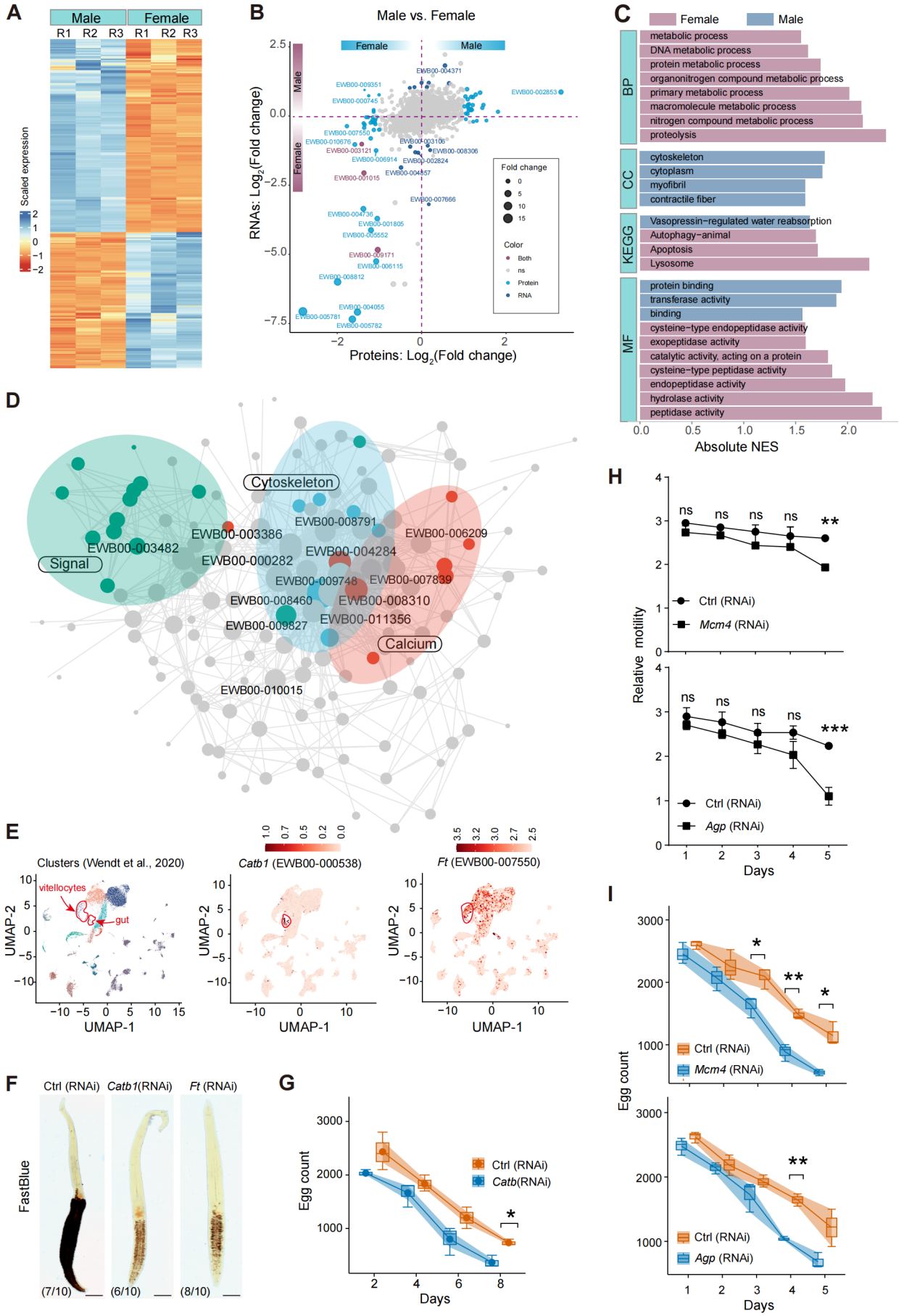
A
Male
Female
R1 R2 R3 R1 R2 R3
Scaled expression
B
Male vs. Female
Female
Male
RNAs: Log2(Fold change)
Proteins: Log2(Fold change)
Fold change
Color
Both
ns
Protein
RNA
C
Female
Male
BP
metabolic process
DNA metabolic process
protein metabolic process
organonitrogen compound metabolic process
primary metabolic process
macromolecule metabolic process
nitrogen compound metabolic process
proteolysis
CC
cytoskeleton
cytoplasm
myofibril
contractile fiber
KEGG
Vasopressin−regulated water reabsorption
Autophagy−animal
Apoptosis
Lysosome
MF
protein binding
transferase activity
binding
cysteine−type endopeptidase activity
exopeptidase activity
catalytic activity, acting on a protein
cysteine−type peptidase activity
endopeptidase activity
hydrolase activity
peptidase activity
Absolute NES
D
Cytoskeleton
Signal
Calcium
EWB00-003482
EWB00-003386
EWB00-000282
EWB00-008791
EWB00-004284
EWB00-006209
EWB00-009748
EWB00-007839
EWB00-008460
EWB00-008310
EWB00-009827
EWB00-011356
EWB00-010015
E
Clusters (Wendt et al., 2020)
vitellocytes
gut
Catb1 (EWB00-000538)
Ft (EWB00-007550)
UMAP-1
UMAP-2
F
Ctrl (RNAi)
Catb1(RNAi)
Ft (RNAi)
FastBlue
(7/10)
(6/10)
(8/10)
G
Egg count
Days
Ctrl (RNAi)
Catb(RNAi)
H
Relative motility
Ctrl (RNAi)
Mcm4 (RNAi)
Agp (RNAi)
Days
I
Egg count
Ctrl (RNAi)
Mcm4 (RNAi)
Agp (RNAi)
Days

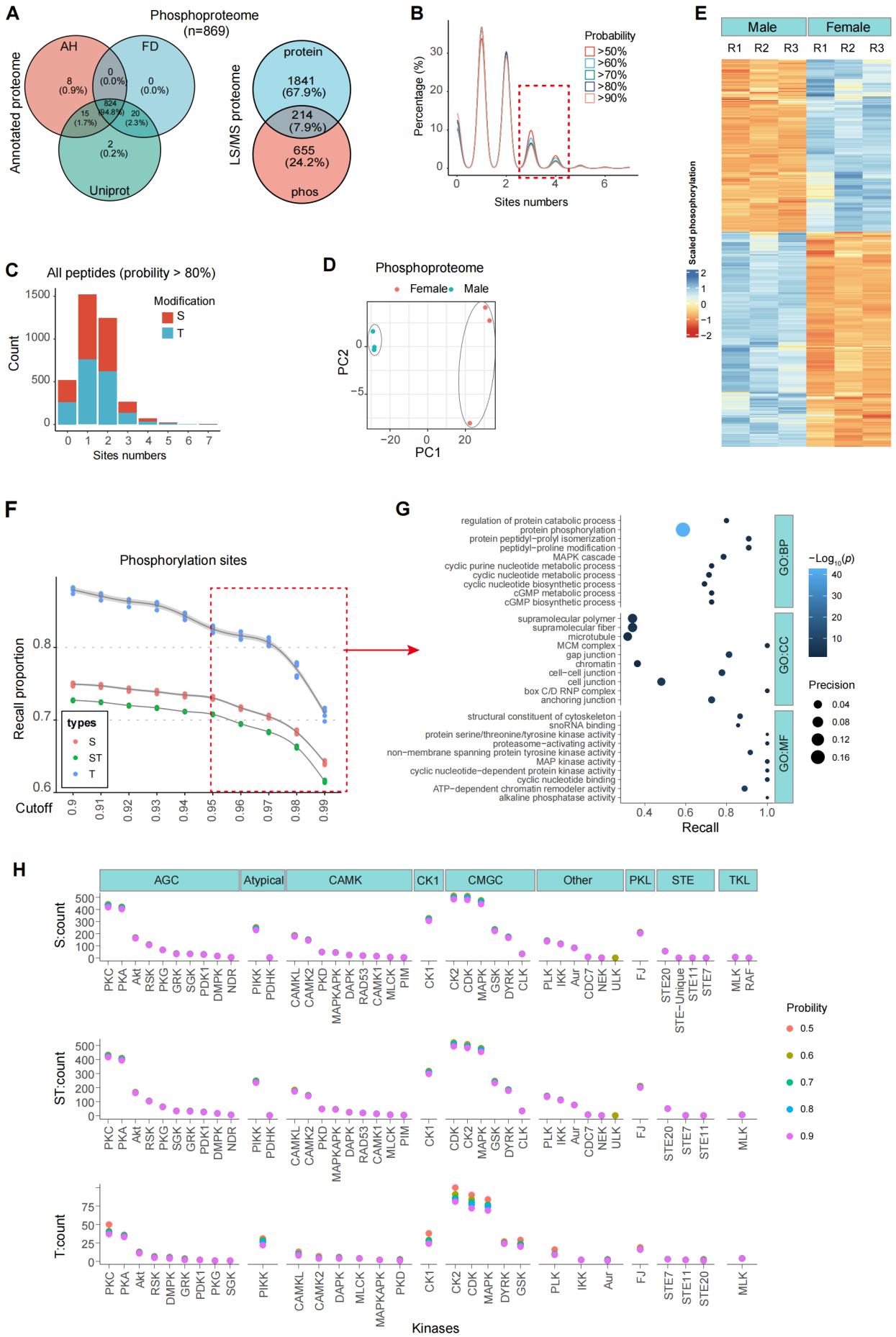
A
Phosphoproteome
(n=869)
Annotated proteome
AH
FD
Uniprot
8
(0.9%)
0
(0.0%)
0
(0.0%)
824
(94.8%)
15
(1.7%)
20
(2.3%)
2
(0.2%)
LS/MS proteome
protein
phos
1841
(67.9%)
214
(7.9%)
655
(24.2%)
B
Probability
>50%
>60%
>70%
>80%
>90%
Percentage (%)
Sites numbers
E
Male
Female
R1
R2
R3
Scaled phosophorylation
C
All peptides (probility > 80%)
Modification
S
T
Count
Sites numbers
D
Phosphoproteome
Female
Male
PC2
PC1
F
Phosphorylation sites
Recall proportion
types
S
ST
T
Cutoff
G
GO:BP
GO:CC
GO:MF
regulation of protein catabolic process
protein phosphorylation
protein peptidyl−prolyl isomerization
peptidyl−proline modification
MAPK cascade
cyclic purine nucleotide metabolic process
cyclic nucleotide metabolic process
cyclic nucleotide biosynthetic process
cGMP metabolic process
cGMP biosynthetic process
supramolecular polymer
supramolecular fiber
microtubule
MCM complex
gap junction
chromatin
cell−cell junction
cell junction
box C/D RNP complex
anchoring junction
structural constituent of cytoskeleton
snoRNA binding
protein serine/threonine/tyrosine kinase activity
proteasome−activating activity
non−membrane spanning protein tyrosine kinase activity
MAP kinase activity
cyclic nucleotide−dependent protein kinase activity
cyclic nucleotide binding
ATP−dependent chromatin remodeler activity
alkaline phosphatase activity
−Log10(p)
Precision
Recall
H
AGC
Atypical
CAMK
CK1
CMGC
Other
PKL
STE
TKL
S:count
ST:count
T:count
Probility
Kinases

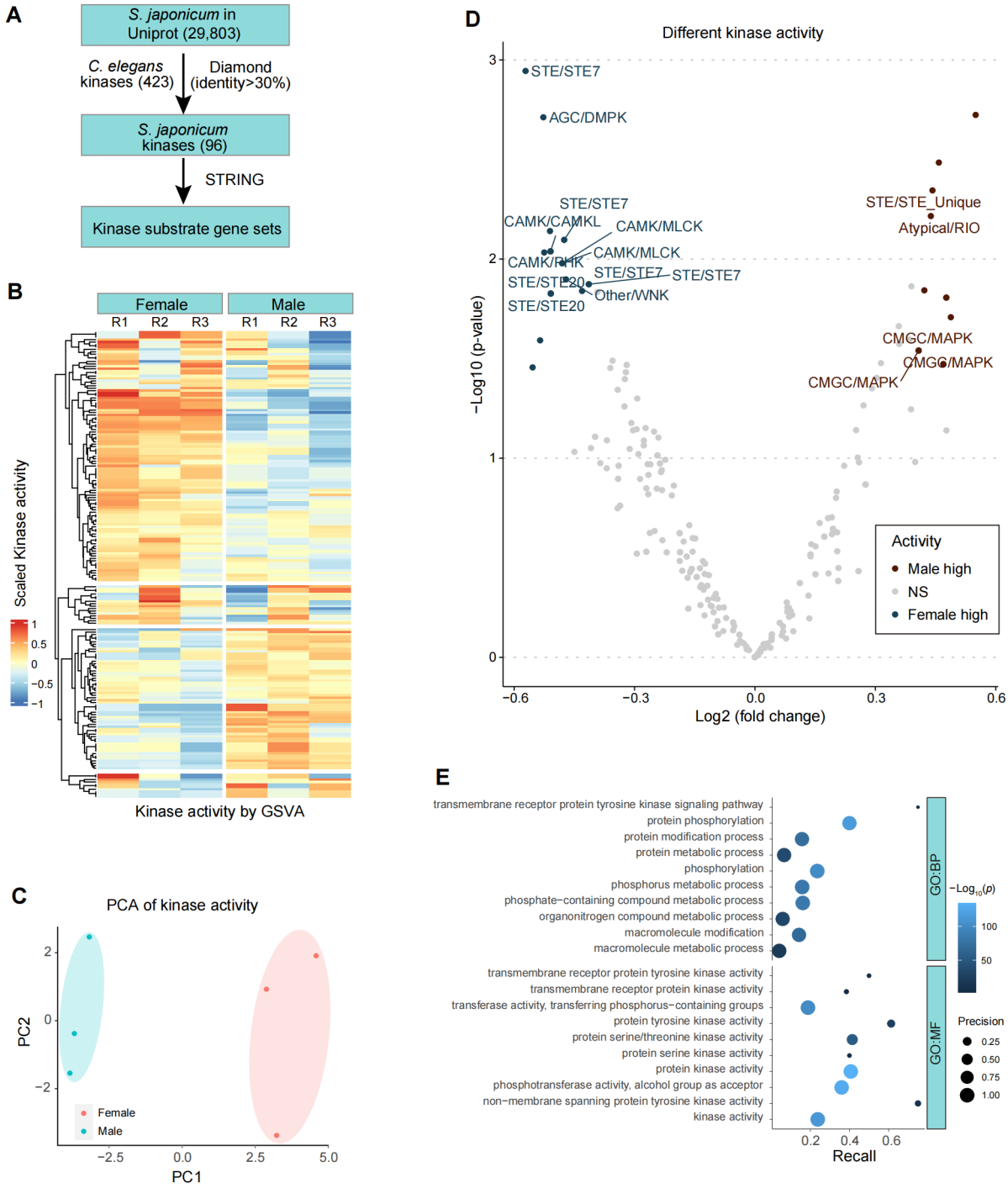
A
S. japonicum in Uniprot (29,803)
C. elegans kinases (423)
Diamond (identity>30%)
S. japonicum kinases (96)
STRING
Kinase substrate gene sets
B
Female
Male
R1 R2 R3 R1 R2 R3
Scaled Kinase activity
1
0.5
0
−0.5
−1
Kinase activity by GSVA
C
PCA of kinase activity
PC2
PC1
Female
Male
D
Different kinase activity
−Log10 (p-value)
Log2 (fold change)
STE/STE7
AGC/DMPK
STE/STE7
CAMK/CAMKL
CAMK/MLCK
CAMK/RIK
CAMK/MLCK
STE/STE20
STE/STE7
STE/STE7
Other/WNK
STE/STE20
STE/STE_Unique
Atypical/RIO
CMGC/MAPK
CMGC/MAPK
CMGC/MAPK
Activity
Male high
NS
Female high
E
transmembrane receptor protein tyrosine kinase signaling pathway
protein phosphorylation
protein modification process
protein metabolic process
phosphorylation
phosphorus metabolic process
phosphate−containing compound metabolic process
organonitrogen compound metabolic process
macromolecule modification
macromolecule metabolic process
transmembrane receptor protein tyrosine kinase activity
transmembrane receptor protein kinase activity
transferase activity, transferring phosphorus−containing groups
protein tyrosine kinase activity
protein serine/threonine kinase activity
protein serine kinase activity
protein kinase activity
phosphotransferase activity, alcohol group as acceptor
non−membrane spanning protein tyrosine kinase activity
kinase activity
GO:BP
GO:MF
−Log10(p)
Precision
Recall

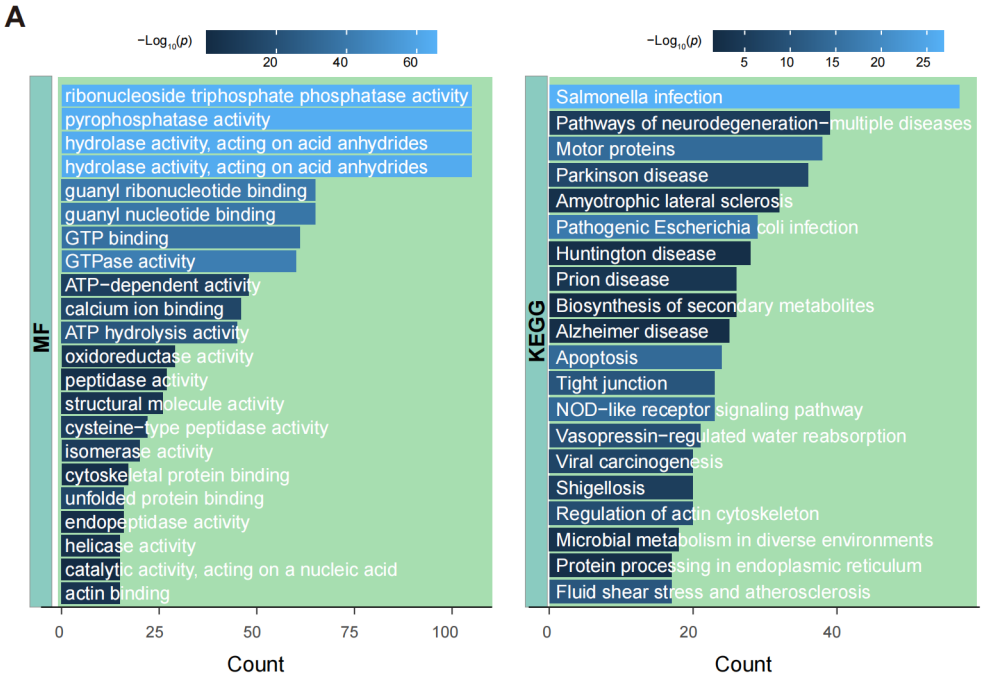
A
−Log10(p)
20
40
60
MF
ribonucleoside triphosphate phosphatase activity
pyrophosphatase activity
hydrolase activity, acting on acid anhydrides
hydrolase activity, acting on acid anhydrides
guanyl ribonucleotide binding
guanyl nucleotide binding
GTP binding
GTPase activity
ATP−dependent activity
calcium ion binding
ATP hydrolysis activity
oxidoreductase activity
peptidase activity
structural molecule activity
cysteine−type peptidase activity
isomerase activity
cytoskeletal protein binding
unfolded protein binding
endopeptidase activity
helicase activity
catalytic activity, acting on a nucleic acid
actin binding
0
25
50
75
100
Count
−Log10(p)
5
10
15
20
25
KEGG
Salmonella infection
Pathways of neurodegeneration−multiple diseases
Motor proteins
Parkinson disease
Amyotrophic lateral sclerosis
Pathogenic Escherichia coli infection
Huntington disease
Prion disease
Biosynthesis of secondary metabolites
Alzheimer disease
Apoptosis
Tight junction
NOD−like receptor signaling pathway
Vasopressin−regulated water reabsorption
Viral carcinogenesis
Shigellosis
Regulation of actin cytoskeleton
Microbial metabolism in diverse environments
Protein processing in endoplasmic reticulum
Fluid shear stress and atherosclerosis
0
20
40
Count

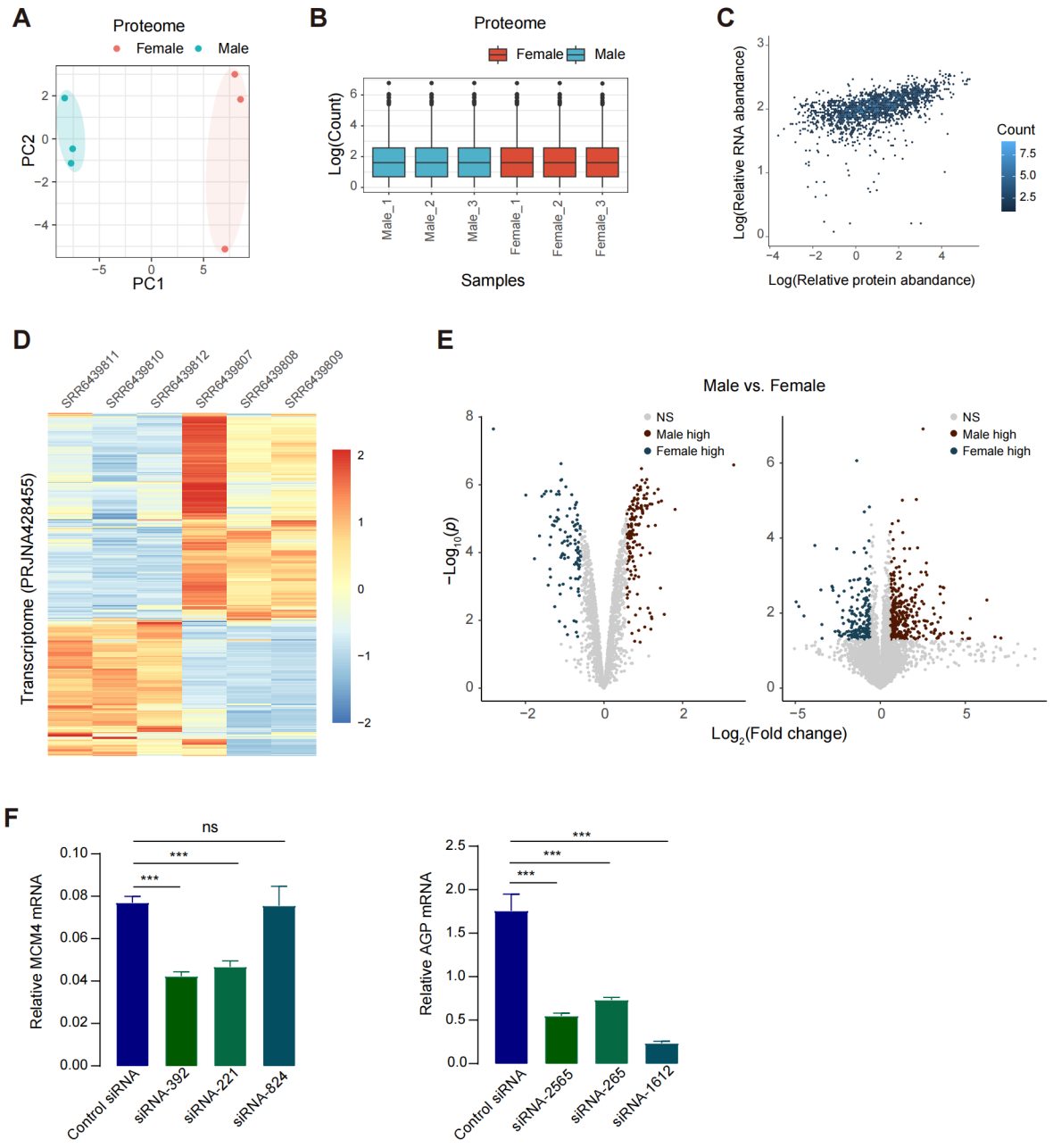
A
Proteome
Female
Male
PC2
PC1
B
Proteome
Female
Male
Log(Count)
Male_1
Male_2
Male_3
Female_1
Female_2
Female_3
Samples
C
Log(Relative RNA abandance)
Log(Relative protein abandance)
Count
7.5
5.0
2.5
D
SRR6439811
SRR6439810
SRR6439812
SRR6439807
SRR6439808
SRR6439809
Transcriptome (PRJNA428455)
E
Male vs. Female
NS
Male high
Female high
−Log10(p)
Log2(Fold change)
F
ns
***
Relative MCM4 mRNA
Control siRNA
siRNA-392
siRNA-221
siRNA-824
Relative AGP mRNA
Control siRNA
siRNA-2565
siRNA-265
siRNA-1612

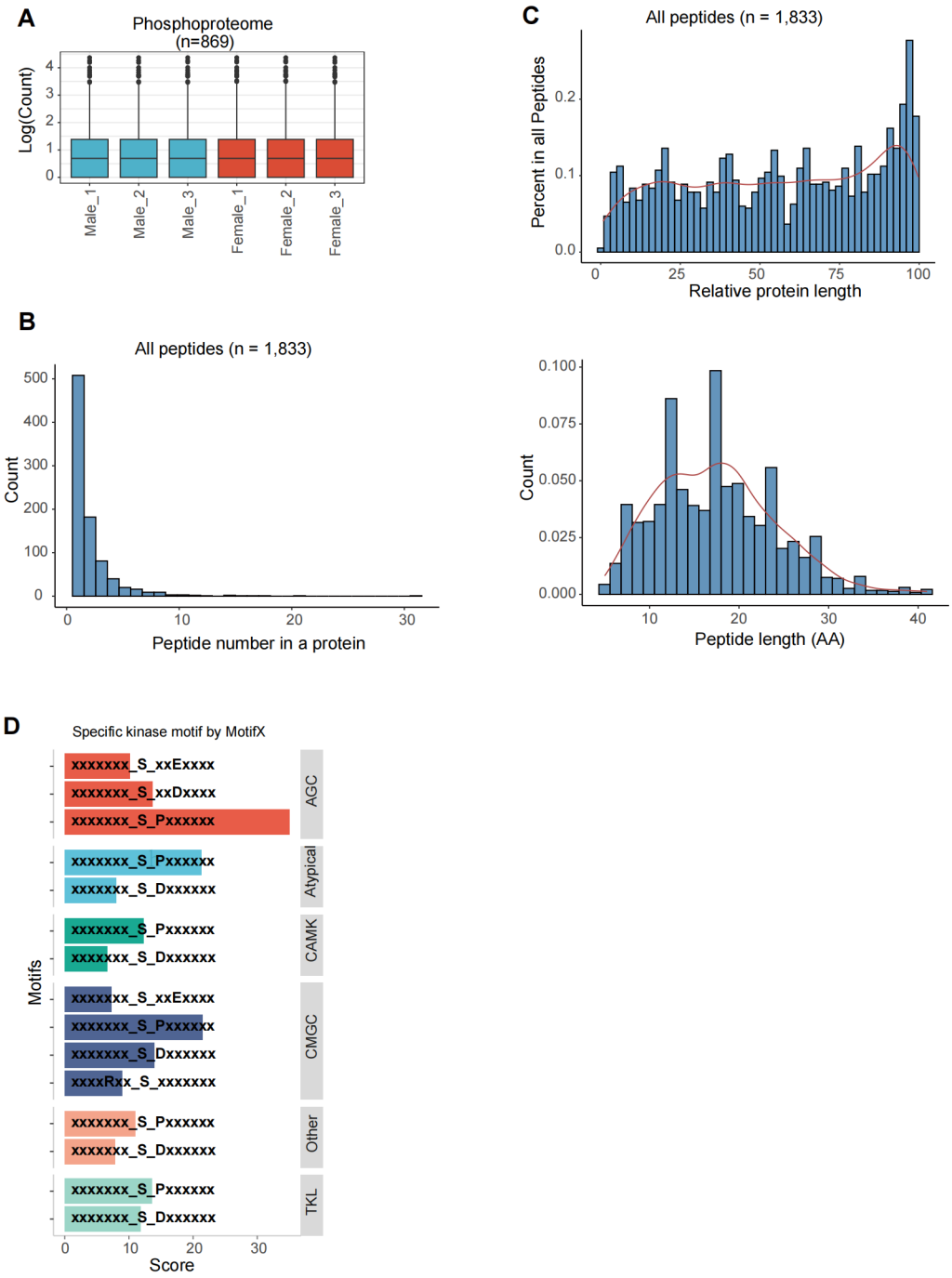
A
Phosphoproteome
(n=869)
Log(Count)
Male_1
Male_2
Male_3
Female_1
Female_2
Female_3
B
All peptides (n = 1,833)
Count
Peptide number in a protein
C
All peptides (n = 1,833)
Percent in all Peptides
Relative protein length
Count
Peptide length (AA)
D
Specific kinase motif by MotifX
Motifs
xxxxxxx_S_xxExxxx
xxxxxxx_S_xxDxxxx
xxxxxxx_S_Pxxxxxx
xxxxxxx_S_Pxxxxxx
xxxxxxx_S_Dxxxxxx
xxxxxxx_S_Pxxxxxx
xxxxxxx_S_Dxxxxxx
xxxxxxx_S_xxExxxx
xxxxxxx_S_Pxxxxxx
xxxxxxx_S_Dxxxxxx
xxxxRxx_S_xxxxxxx
xxxxxxx_S_Pxxxxxx
xxxxxxx_S_Dxxxxxx
xxxxxxx_S_Pxxxxxx
xxxxxxx_S_Dxxxxxx
AGC
Atypical
CAMK
CMGC
Other
TKL
Score

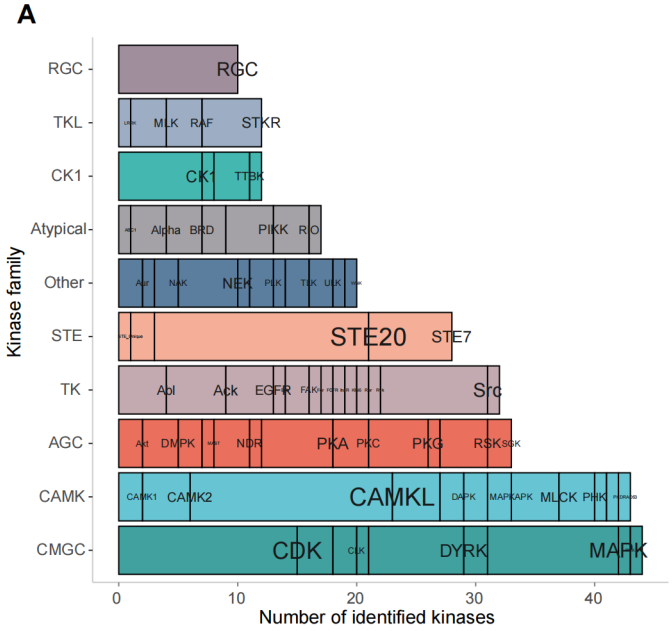
A
RGC
TKL
CK1
Atypical
Other
STE
TK
AGC
CAMK
CMGC
Kinase family
RGC
MLK
RAF
STKR
CK1
TTBK
Alpha
BRD
PIKK
RIO
NAK
NEK
PEK
TBK
ULK
STE20
STE7
Abl
Ack
EGFR
Src
DMPK
NDR
PKA
PKC
PKG
RSK
SGK
CAMK1
CAMK2
CAMKL
DAPK
MAPKAPK
MLCK
PHK
CDK
DYRK
MAPK
0
10
20
30
40
Number of identified kinases